nagra.

Arbeitsbericht NAB 22-03

TBO Rheinau-1-1: Data Report

Dossier VI Wireline Logging and Micro-hydraulic Fracturing

June 2023

J. Gonus, E. Bailey, J. Desroches & R. Garrard

National Cooperative
for the Disposal of
Radioactive Waste

Hardstrasse 73
P.O. Box
5430 Wettingen
Switzerland
Tel. +41 56 437 11 11

nagra.ch

nagra.

Arbeitsbericht NAB 22-03

TBO Rheinau-1-1: Data Report

Dossier VI Wireline Logging and Micro-hydraulic Fracturing

June 2023

J. Gonus[1], E. Bailey[1], J. Desroches[1] & R. Garrard[2]

[1] Ad Terra Energy
[2] Nagra

Keywords:
RHE1-1, Zürich Nordost, TBO, deep drilling campaign, wireline logging, petrophysical logging, in-situ testing, micro-hydraulic fracturing

National Cooperative for the Disposal of Radioactive Waste

Hardstrasse 73
P.O. Box
5430 Wettingen
Switzerland
Tel. +41 56 437 11 11

nagra.ch

Nagra Arbeitsberichte ("Working Reports") present the results of work in progress that have not necessarily been subject to a comprehensive review. They are intended to provide rapid dissemination of current information.

This NAB aims at reporting drilling results at an early stage. Additional borehole-specific data will be published elsewhere.

In the event of inconsistencies between dossiers of this NAB, the dossier addressing the specific topic takes priority. In the event of discrepancies between Nagra reports, the chronologically later report is generally considered to be correct. Data sets and interpretations laid out in this NAB may be revised in subsequent reports. The reasoning leading to these revisions will be detailed there.

This Dossier was prepared by a project team consisting of:
J. Gonus (petrophysics QC, theoretical concepts and log analysis)
E. Bailey (introductory chapters, BHI QC and project management)
J. Desroches (MHF QC and theoretical concepts)
R. Garrard (coordination and QC review)

Editorial work: P. Blaser and M. Unger

Petrophysical log graphic files were created using Geolog Emerson E&P Software - Emerson Paradigm and Terrastation.

The Dossier has greatly benefitted from reviews by external and internal experts. Their input and work are very much appreciated.

Table of Contents

List of Tables

List of Figures

List of Appendices

Note: The Appendices A – C are only included in the digital version of this report and can be found under the paper clip symbol.

1 Introduction

1.1 Context

To provide input for site selection and the safety case for deep geological repositories for radioactive waste, Nagra has drilled a series of deep boreholes ("Tiefbohrungen", TBO) in Northern Switzerland. The aim of the drilling campaign is to characterise the deep underground of the three remaining siting regions located at the edge of the Northern Alpine Molasse Basin (Fig. 1-1).

In this report, we present the results from the Rheinau-1-1 borehole located in the siting region Zürich Nordost (Fig. 1-2). In the following, the unique exploration objective of this specific borehole is further outlined.

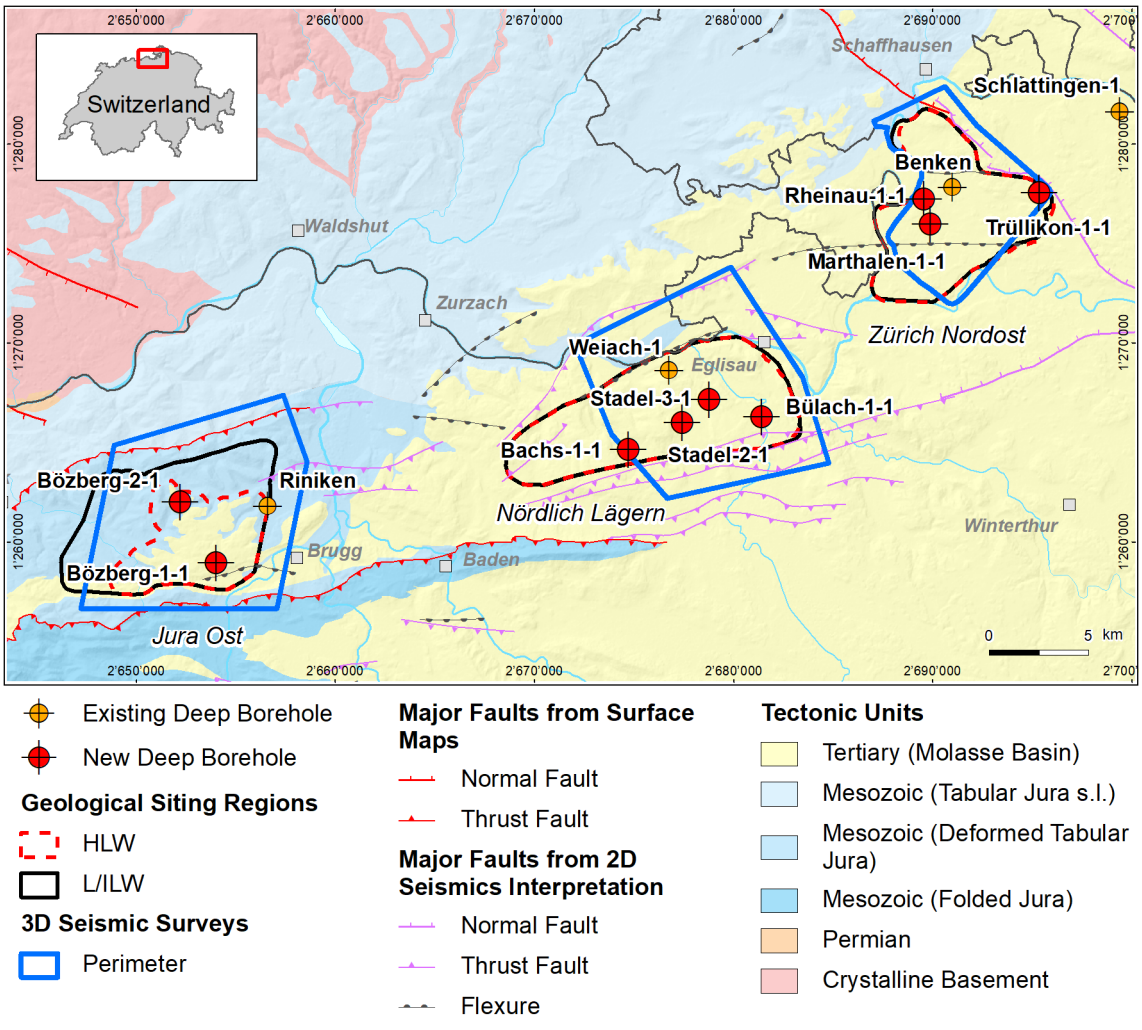

Fig. 1-1: Tectonic overview map with the three siting regions under investigation

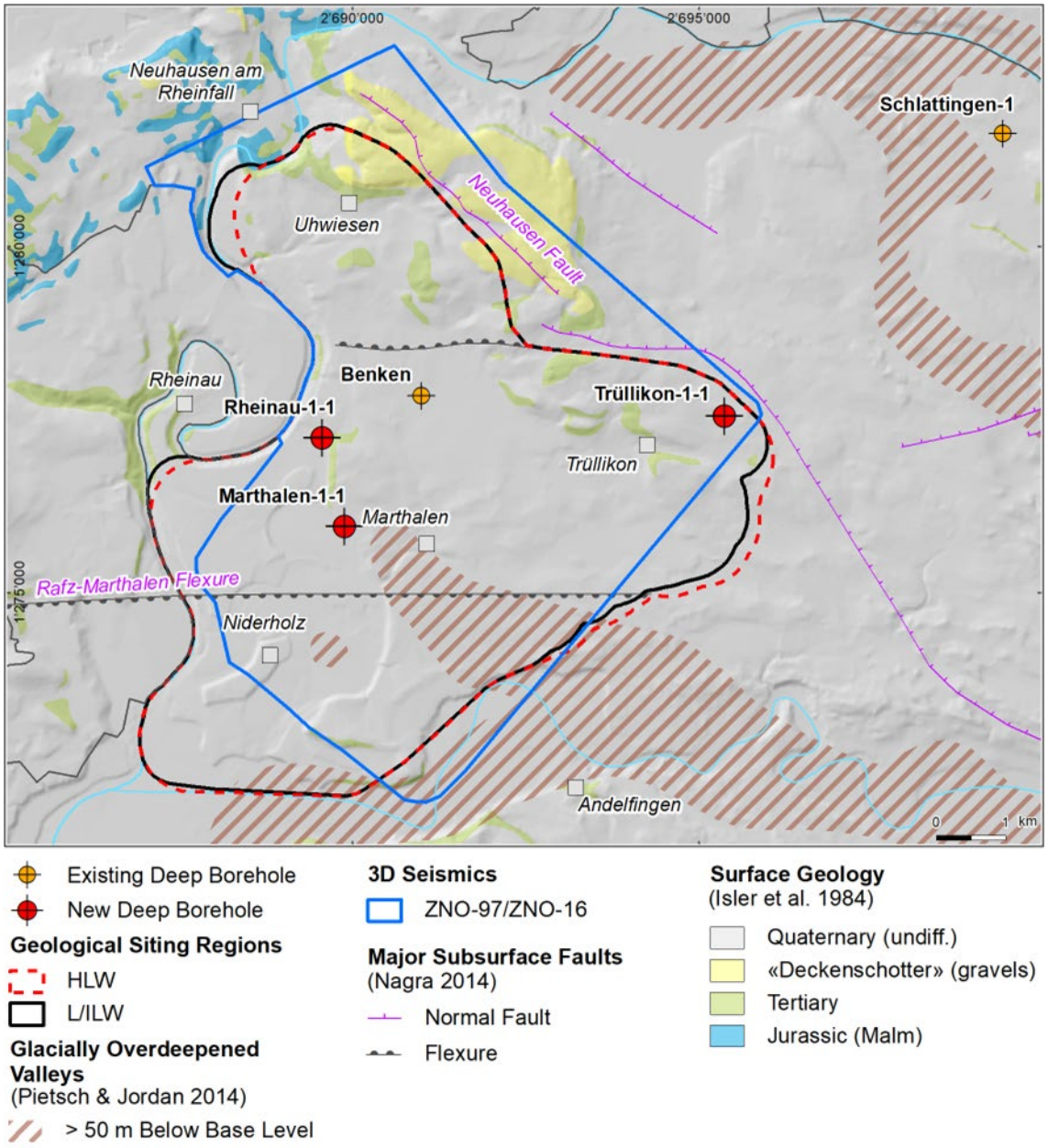

Fig. 1-2: Overview map of the investigation area in the Zürich Nordost siting region with the location of the RHE1-1 borehole in relation to the Benken, TRU1-1 and MAR1-1 boreholes

Exploration objective of the Rheinau-1-1 borehole

In the context of Nagra's TBO project, the Rheinau-1-1 (RHE1-1) borehole is the only deviated borehole. It was planned as a case study with the primary objective of characterising the structural geology of the Opalinus Clay in the area of a steeply dipping fault. Furthermore, dedicated hydrological packer testing and investigations of natural tracers in porewater were conducted to investigate the self-sealing capacity of the Opalinus Clay. More specifically, a stepped constant head injection test was performed in addition to the standard hydraulic packer test to investigate the evolution of transmissivity as a function of effective stress in a fractured interval (*cf.* Dossier VII, Hydraulic Packer Testing for details).

To enable hydraulic testing in the Opalinus Clay with its relatively low strength and high swelling capacity, the maximum borehole deviation (with respect to vertical) was limited to approximately 35° (borehole plunge of 55°). Hence, for the absolute deviation, a trade-off had to be made between maximising the lateral coverage for fracture frequency statistics (large deviation desired) and robust in-situ testing (small deviation desired).

Given the above-outlined scientific goals and related technical requirements, the Rheinau Fault, located immediately east of the Rheinau-1 drill site, was selected for this case study. It is an NNE-SSW trending, steeply dipping fault showing only very minor indications of vertical offsets in seismic amplitude sections. Nevertheless, it was already identified in seismic attribute horizon slices during initial interpretation of Nagra's 3D seismic campaign in the Zürich Nordost siting region (Birkhäuser et al. 2001) and later confirmed during the analysis of follow-up seismic processing products (e.g. Nagra 2019). Fig. 1-3 shows that this fault has a clear seismic attribute expression along the boundaries of the formations below the Opalinus Clay and also along some of the more brittle units above (see horizon slices of the Top Bänkerjoch and Top Villigen Formations shown in Fig. 1-3). However, within the Opalinus Clay, no clear seismic expression is observed. Fig. 1-4 shows the 3D seismic interpretation considered for trajectory planning of the RHE1-1 borehole together with the discussed and executed borehole trajectories.

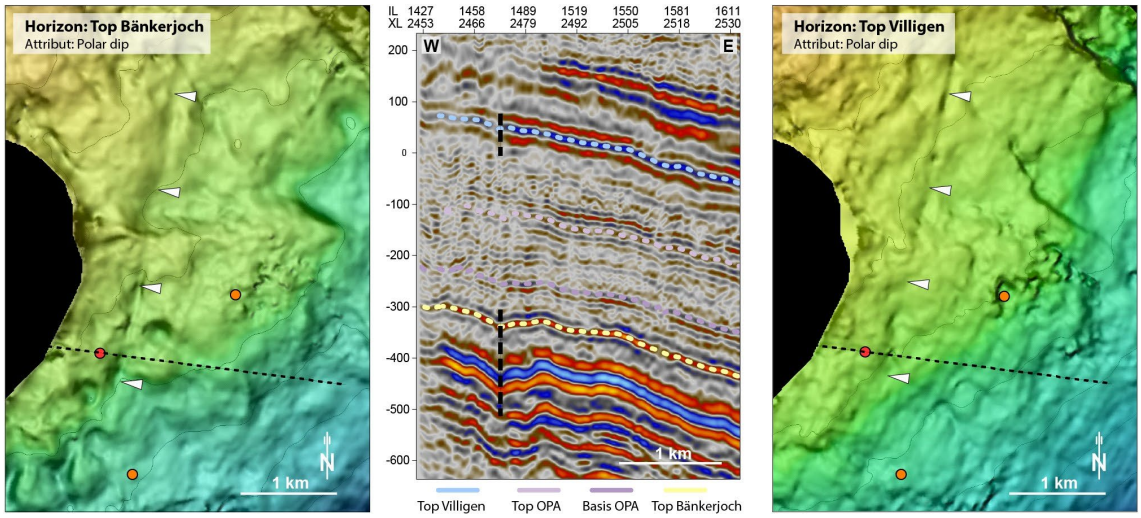

Fig. 1-3: Seismic amplitude cross-section and seismic attribute maps showing the Rheinau Fault

Left and right panels: Seismic attribute maps (polar dip) of a depth-migrated seismic cube (PSDM-A) overlain with depth values (yellowish and blueish colors indicate shallower and larger depths, respectively). The dashed black line indicates the position of the seismic section shown in the central panel. Red and orange dots show the position of the RHE1-1 borehole and neighouring boreholes, respectively. White trianlges mark the lineament representing the Rheinau Fault.

Central panel: Corresponding seismic amplitude section crossing the Rheinau Fault. The vertical axis indicates depth above sea level, and the horizontal axis shows the inline and crossline positions. The approximate trace of the Rheinau Fault above and below the Opalinus Clay is indicated by dashed black lines.

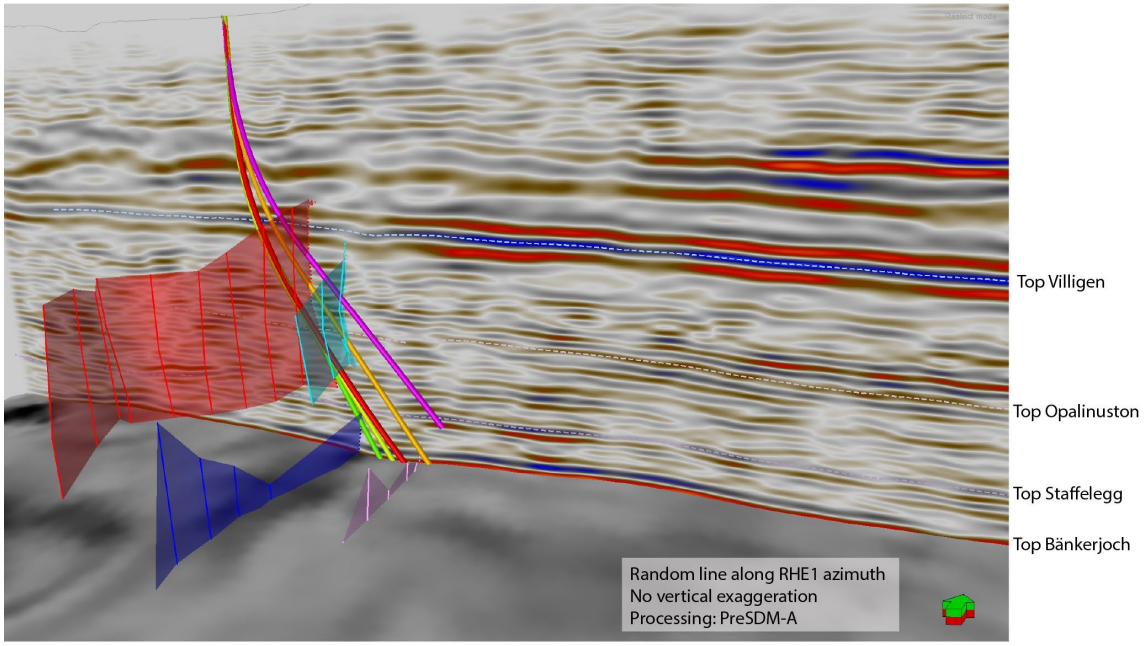

Fig. 1-4: Detailed seismic fault interpretation available for trajectory planning and discussed/ executed well trajectories

Cross-section shows seismic amplitude (seismic processing: pre-stack depth migration PDSM-A). The north direction is indicated by a green-and-red arrow. The vertical distance between the Top Opalinus Clay and Top Staffelegg is ~ 120 m and shows no vertical exaggeration. The horizon slice shows polar dip attribute. Semitransparent subvertical surfaces indicate intepreted faults. The final planned and the drilled trajectories are shown in light green and red, respectively. Other discussed trajectories are shown in yellow, orange and red.

Fig. 1-5 shows a conceptual structural model for the Rheinau Fault incorporating both 3D seismic interpretations and observations from other exploration boreholes as well as from outcrop studies. This conceptual model shows a pronounced mechanical stratigraphy of Northern Switzerland's Mesozoic sedimentary sequence with more focused deformation in the competent units, and distributed deformation in the incompetent units (Roche et al. 2020). Prior to drilling, three hypotheses were formulated on what the RHE1-1 borehole is likely to encounter in the Opalinus Clay. These hypotheses ranged from 1) absence of a distinct fault zone, likely due to a strong degree of strain partitioning within the rheologically weak Opalinus Clay, 2) one or several prominent fault zones, for example revealing cataclastic fault rock or scaly clay as it has been described to occur along larger faults within the Opalinus Clay (Jäggi et al. 2017) and 3) the former but including the occurrence of secondary mineralisations.

As this report represents a data documentation, it deliberately avoids engaging in a synthesis of the observations and test results. Nevertheless, the following results can already be highlighted:

- The drilled trajectory was within close limits compared to the planned well path (see Dossier I for a detailed comparison).
- The borehole did not yield any evidence of a larger-scale fault zone within the Opalinus Clay. However, a number of fault planes have been encountered (*cf.* Dossier V).
- In-situ hydraulic packer tests across these features (*cf.* Dossier VII) yielded hydraulic conductivities similar to undisturbed Opalinus Clay.

- The stepped constant head test demonstrated that a significant enhancement of the flow rate can only be achieved in existing fractures if the fluid pressure is raised considerably and the magnitude of elevated fluid pressure can be maintained (*cf.* Dossier VII).
- Excursions in the profiles of natural tracers can indicate past fluid flow. No such irregularities are seen for the RHE1-1 borehole in the Opalinus Clay (*cf.* Dossier VIII). The stable isotope porewater profiles show characteristics similar to the neighouring vertical boreholes MAR1-1 and Benken.

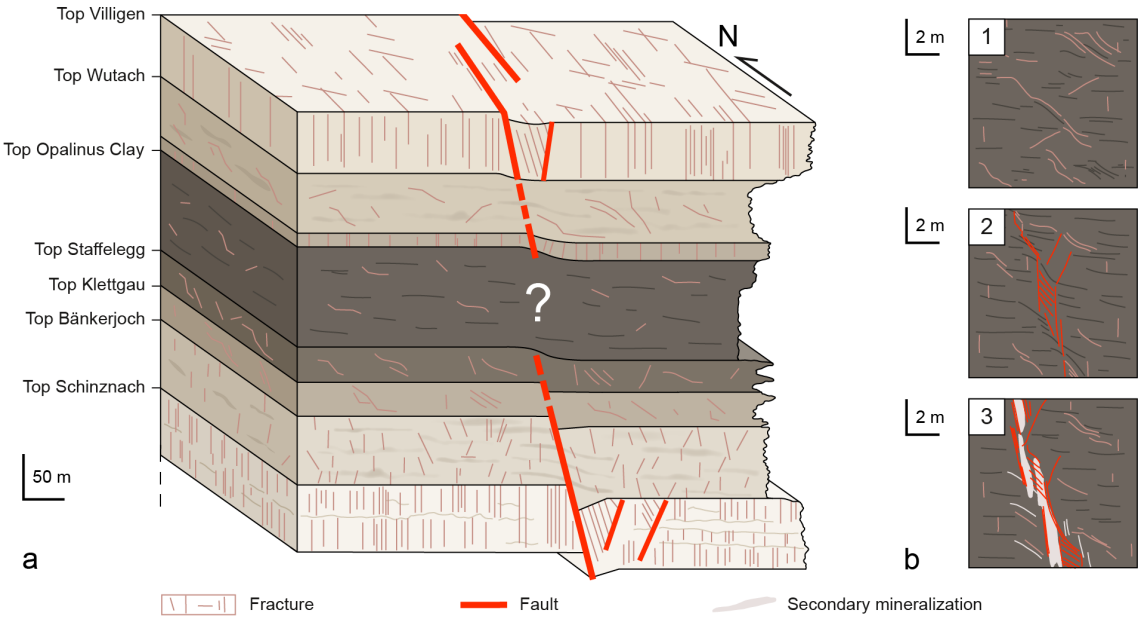

Fig. 1-5: Conceptual structural model of the Rheinau Fault

(a) Conceptual block model. The pronounced mechanical stratigraphy of the Mesozoic sequence in the area is stressed via a schematic weathering profile. The RHE1-1 borehole aimed at characterising the deformation style in the Opalinus Clay constituting a mechanically weak layer in between rheologically stiffer units (e.g. under- and overlying Schinznach/Bänkerjoch and Villigen/Wutach Formations). According to outcrop records and previous borehole results, these units show a significantly higher frequency of fault planes compared to the Opalinus Clay. In 3D seismics, the Rheinau Fault is also only clearly recognisable at the horizons related to stiffer formations.

(b) Hypothetic deformation characteristics of the Opalinus Clay to be encountered in the RHE1-1 borehole: 1) No exceptional deformation features besides small-scale fault planes as previously observed in vertical boreholes outside of seismically recognised faults. 2) One or several localised zones associated with cataclastic fault rock (e.g. scaly clay) as described for larger fault zones elsewhere (e.g. Jäggi et al. 2017). 3) The above, but also including secondary mineralisation (not to scale on picture).

1.2 Location and specifications of the borehole

The Rheinau-1-1 (RHE1-1) exploratory borehole is the eighth borehole drilled within the framework of the TBO project. The drill site is located in the western part of the Zürich Nordost siting region (Fig. 1-2). The deviated borehole reached a final depth of 827.99 m MD = 745.33 m TVD (true vertical depth)[1]. The borehole specifications are provided in Tab. 1-1.

Tab. 1-1: General information about the RHE1-1 borehole

Siting region	Zürich Nordost
Municipality	Rheinau (Canton Zürich / ZH), Switzerland
Drill site	Rheinau-1 (RHE1)
Borehole	Rheinau-1-1 (RHE1-1)
Coordinates	LV95: 2'689'563.92 / 1'277'235.06
Elevation	Ground level = top of rig cellar: 387.23 m above sea level (asl)
Borehole depth	827.99 m measured depth (MD) = 745.33 m true vertical depth (TVD) below ground level (bgl)
Borehole deviation at total depth (TD)	Inclination from vertical: 38.93° Azimuth from North: 76.25°
Drilling period	19th July – 10th October 2021 (spud date to end of rig release)
Drilling company	PR Marriott Drilling Ltd
Drilling rig	Rig-16 Drillmec HH102
Drilling fluid	Water-based mud with various amounts of different components such as[2]: …0 – 497 m: Polymers 497 – 828 m: Potassium silicate & polymers

The lithostratigraphic profile and the casing scheme are shown in Fig. 1-6. The comparison of the core versus log depth[3] of the main lithostratigraphic boundaries in the RHE1-1 borehole is shown in Tab. 1-2.

[1] Measured depth (MD) refers to the position along the borehole trajectory, starting at ground level, which for this borehole is the top of the rig cellar. For a perfectly vertical borehole, MD below ground level (bgl) and true vertical depth (TVD) are the same. In all Dossiers depth refers to MD unless stated otherwise.

[2] For detailed information see Dossier I.

[3] Core depth refers to the depth marked on the drill cores. Log depth results from the depth observed during geophysical wireline logging. Note that the petrophysical logs have not been shifted to core depth, hence log depth differs from core depth.

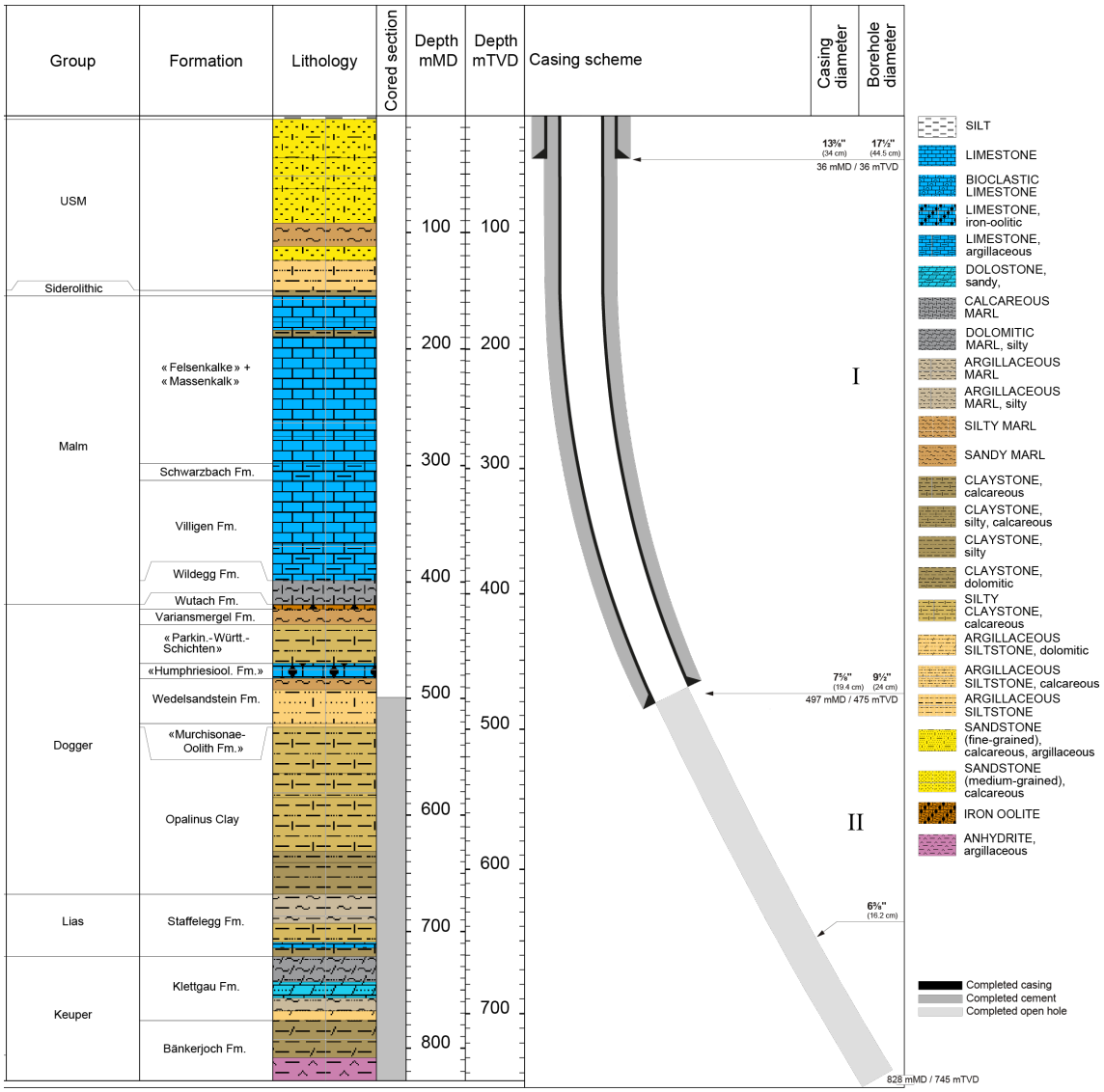

Fig. 1-6: Lithostratigraphic profile and casing scheme for the RHE1-1 borehole[4]

[4] For detailed information see Dossier I and III.

Tab. 1-2: Core and log depth for the main lithostratigraphic boundaries in the RHE1-1 borehole[5]

System / Period	Group	Formation	Core top depth in m (MD)	Log top depth in m (MD)		Core top depth in m (TVD)	Log top depth in m (TVD)	
Quaternary			**3**		—	**3**		–
Paleogene + Neogene	USM		149.90		—	149.88		–
	Siderolithic		**154.40**		—	**154.37**		–
Jurassic	Malm	«Felsenkalke» + «Massenkalk»	298.10		—	295.71		–
		Schwarzbach Formation	312.70		—	309.70		–
		Villigen Formation	398.80		—	389.75		–
		Wildegg Formation	419.20		—	408.04		–
	Dogger	Wutach Formation	423.40		—	411.78		–
		Variansmergel Formation	436.60		—	423.47		–
		«Parkinsoni-Württembergica-Sch.»	469.80		—	452.23		–
		«Humphriesioolith Formation»	482.80		—	463.20		–
		Wedelsandstein Formation	521.43	521.21	—	495.83	495.64	–
		«Murchisonae-Oolith Formation»	524.61	524.33	—	498.51	498.27	–
		Opalinus Clay	668.07	668.19	—	617.65	617.75	–
	Lias	Staffelegg Formation	**721.46**	**721.50**	—	**660.95**	**660.98**	–
Triassic	Keuper	Klettgau Formation	776.42	776.79	—	704.82	705.11	–
		Bänkerjoch Formation final depth	827.99	828.24		745.33	745.52	

[5] For details regarding lithostratigraphic boundaries see Dossier III and IV; for details about depth shifts (core goniometry) see Dossier V.

1.3 Documentation structure for the RHE1-1 borehole

NAB 22-03 documents the majority of the investigations carried out in the RHE1-1 borehole, including laboratory investigations on core material. The NAB comprises a series of stand-alone dossiers addressing individual topics and a final dossier with a summary composite plot (Tab. 1-3).

This documentation aims at early publication of the data collected in the RHE1-1 borehole. It includes most of the data available approximately one year after completion of the borehole. Some analyses are still ongoing and results will be published in separate reports.

The current borehole report will provide an important basis for the integration of datasets from different boreholes. The integration and interpretation of the results in the wider geological context will be documented later in separate geoscientific reports.

Tab. 1-3: List of dossiers included in NAB 22-03

Black indicates the dossier at hand.

Dossier	Title	Authors
I	TBO Rheinau-1-1: Drilling	M. Ammen & P.-J. Palten
II	TBO Rheinau-1-1: Core Photography	D. Kaehr & M. Gysi
III	TBO Rheinau-1-1: Lithostratigraphy	M. Schwarz, P. Schürch, P. Jordan, H. Naef, R. Felber, T. Ibele & F. Casanova
IV	TBO Rheinau-1-1: Microfacies, Bio- and Chemostratigraphic Analysis	S. Wohlwend, H.R. Bläsi, S. Feist-Burkhardt, B. Hostettler, U. Menkveld-Gfeller, V. Dietze & G. Deplazes
V	TBO Rheinau-1-1: Structural Geology	A. Ebert, S. Cioldi, E. Hägerstedt, L. Gregorczyk & F. Casanova
VI	TBO Rheinau-1-1: Wireline Logging and Micro-hydraulic Fracturing	J. Gonus, E. Bailey, J. Desroches & R. Garrard
VII	TBO Rheinau-1-1: Hydraulic Packer Testing	R. Schwarz, M. Willmann, P. Schulte, H. Fisch, S. Reinhardt, L. Schlickenrieder, M. Voß & A. Pechstein
VIII	TBO Rheinau-1-1: Rock Properties and Natural Tracer Profiles	J. Iannotta, F. Eichinger, L. Aschwanden & D. Traber
IX		
X	TBO Rheinau-1-1: Petrophysical Log Analysis	S. Marnat & J.K. Becker
	TBO Rheinau-1-1: Summary Plot	Nagra

1.4 Scope and objectives of this dossier

The dossier at hand describes the acquisition, quality control and results of the Petrophysical Logging (PL) measurements in the RHE1-1 borehole.

Petrophysical log measurements were acquired in open borehole conditions (no casing) with wireline conveyed logging tools to determine continuous profiles across the borehole of physical and chemical properties of the formation, including its mineralogy, clay types, porosity, fluid content, and acoustic properties. Petrophysical logs were further acquired to obtain high-resolution circumferential images of the borehole wall, as well as to measure borehole physical parameters such as its geometry, mud resistivity and mud temperature.

A series of in situ stress measurements were planned using the micro-hydraulic fracturing technique to estimate the orientation and magnitude of the earth stress at different depths. The objectives of the MHF testing programme were to determine if the presence of a discontinuity in the Opalinus Clay potential rock host induced any changes in the stress field and provide calibration points for mechanical earth models (MEM) of the rock mass (both 1D and 3D). As a result of the borehole conditions encountered (azimuth close to that of σ_h and deviation around 38°), no MHF testing was attempted in RHE1-1.

All PL was performed by the wireline logging company Schlumberger (SLB). Ad Terra Energy (formerly Geneva Petroleum Consultants International) were responsible for planning wireline operations, technical supervision at the worksite, quality assurance and control (QA-QC) of data, database management and general wireline logging support.

This dossier is organised as follows:

- Chapter 2: The sequence of events for PL and associated log / data coverage is provided.
- Chapter 3: The QA-QC procedure used to assess the quality of the petrophysical logs is detailed. A continuous profile of each log across the entire measured depth of the borehole is quality-controlled, corrected and spliced together to generate a quality-controlled composite log. The results of the composite log are discussed. The composite log will then be used as the final log data for input into further data analysis processes such as formation evaluation (e.g. Stochastic Petrophysical Log Analysis described in Dossier X), calibration with seismic data and integration with sedimentology and structural geology data (from cores, cuttings, adjacent boreholes and regional geology).
- Chapter 4: Although Borehole Imagery (BHI) logs were acquired as a part of the petrophysical logging, the objectives of BHI are related to Structural Geology (analysis of image features described in Dossier V) and MHF. Thus, even if no MHF was finally attempted in the RHE1-1 borehole, the QC, processing and interpretation processes of BHI are described in a chapter separate from the QA-QC procedures of the other petrophysical logs in Chapter 3.
- Chapter 5: Justifications for not attempting MHF in RHE1-1 are provided.
- Finally, this report includes a set of appendices, where spliced PL data can be found.

2 Wireline logging and testing operations

The RHE1-1 borehole was planned in 2 drilling sections. After installation of the 13⅜" outer diameter (OD) conductor casings, Section I was drilled with the 9½" drill bit and petrophysical logs acquired over the entire section before installation of the 7⅝" casing. Section II was cored in two parts with the 6⅜" core bit and a gyro run after section part to ensure the trajectory of the well was maintained. Once section TD was reached, petrophysical logs were acquired continuously over the entire section, before the borehole was backfilled with cement up from 827.99 m MD to surface. Detailed descriptions of the borehole design and mud conditions at the time of logging and testing are included in the Excel Composite Report (Appendix A), under the worksheets entitled 'Borehole design' and 'Hole & mud system'. Additional details about borehole configuration, casing and cementing scheme and mud parameters can be found in Dossier I.

Wireline logging and testing operations in RHE1-1 were divided into the following groups of activities:

- Petrophysical Logging (PL)
- *Technical Logging (TL)*
- *Vertical Seismic Profiling (VSP)*

Petrophysical logs are continuous measurements (normally recorded every half foot or approximately 15 cm) of mineralogy and physical properties of formation rocks, their contained fluids, and the borehole environment between the wireline conveyed logging tool sensors and the borehole wall. Petrophysical logs were acquired with conventional and advanced wireline-conveyed logging tools. Conventional tools measured Depth (measured depth [MD], or log depth, that is the depth reference for all wireline measurements), Total Gamma Ray (naturally occurring gamma radiation), Spontaneous Potential (electric potential difference between the formation and an electrode at surface), Temperature, Caliper (measurement of the borehole diameter), Inclinometer (measurement of the borehole trajectory), as well as the standard "quad combo" tools: Resistivity (electrical resistivity at different depths of investigation in the formation), Sonic (compressional and shear wave slowness), Density (measurement of the bulk density and the photoelectric factor), and Neutron (measurement of the neutron hydrogen index, a proxy of porosity, as well as the sigma capture cross-section). Advanced tools measured the Spectral Gamma Ray (potassium, thorium and uranium contributions to the total naturally occurring gamma radiation), Elemental Spectroscopy, and Microresistivity and Ultrasonic borehole images. These logging tools and their main measurements are described in detail in the subsequent Chapter 3 – Petrophysical Logging and Chapter 4 – Borehole Imagery.

As well as PL, wireline operations also included Technical Logging (TL) and Vertical Seismic Profiling (VSP). TL acquired data on the physical properties of the open borehole (geometry and trajectory) and the permanent casing installation. The borehole geometry was measured using calipers for both assessing the borehole condition (breakouts / wash-outs present) and determining the volume of cement needed for casing installations. The borehole inclination and azimuth were measured to confirm the borehole trajectory. To assess the quality of the cement behind the casing, Cement Bond Logs (CBL) and acoustic impedance logs were acquired using sonic (MSIP) and ultrasonic imaging (USIT) tools. Borehole deviation surveys, cement volume calculations and CBL logs are described in Dossier I. VSP acquired high resolution borehole seismic measurements used for correlation with, and enhancement of, surface seismic data. VSP will be addressed in a separate document. TL and VSP are not described further in this report.

A summary of all wireline logging and testing activities carried out in the RHE1-1 borehole is given in Tab. 2-1. Fig. 2-1 depicts graphically the log coverage for PL. 2 PL campaigns were undertaken, covering all sections of the RHE1-1 borehole. No MHF testing was attempted as the azimuth and orientation of the borehole would not have provided useable data. A more detailed analysis of the log measurement coverage is provided in Chapter 3.

Details of the logging runs, logging dates, wireline logging company, logging interval, logging suite and principal measurements acquired for PL operations are provided in Tab. 2-2. Mnemonics for each tool in the logging suite listed in this table are given in Tab. 2-3.

Tab. 2-1: Logging and testing activities during drilling of the RHE1-1 borehole

Drilling phase / section	**Permanent casing size at time of logging** **Casing / liner shoe depth**	**Open hole interval and bit size**	**Start date**	**End date**	**Coring**	**Technical logging**	**Petrophysical logging**	**Micro-hydraulic fracturing**	**Vertical seismic profiling**
I	13⅜" 2.42 to 35.80 m MD	35.80 to 497.00 m in 9½"	19.07.2021	29.07.2021		×	×		
II	7⅝" 1.97 to 496.13 m MD	497.00 to 499.10 in 6½" 499.10 to 606.00 in 6⅜"	30.07.2021	05.08.2021	×	×			
		497.00 to 499.10 in 6½" 499.10 to 827.99 in 6⅜"	05.08.2021	05.10.2021	×	×	×		×

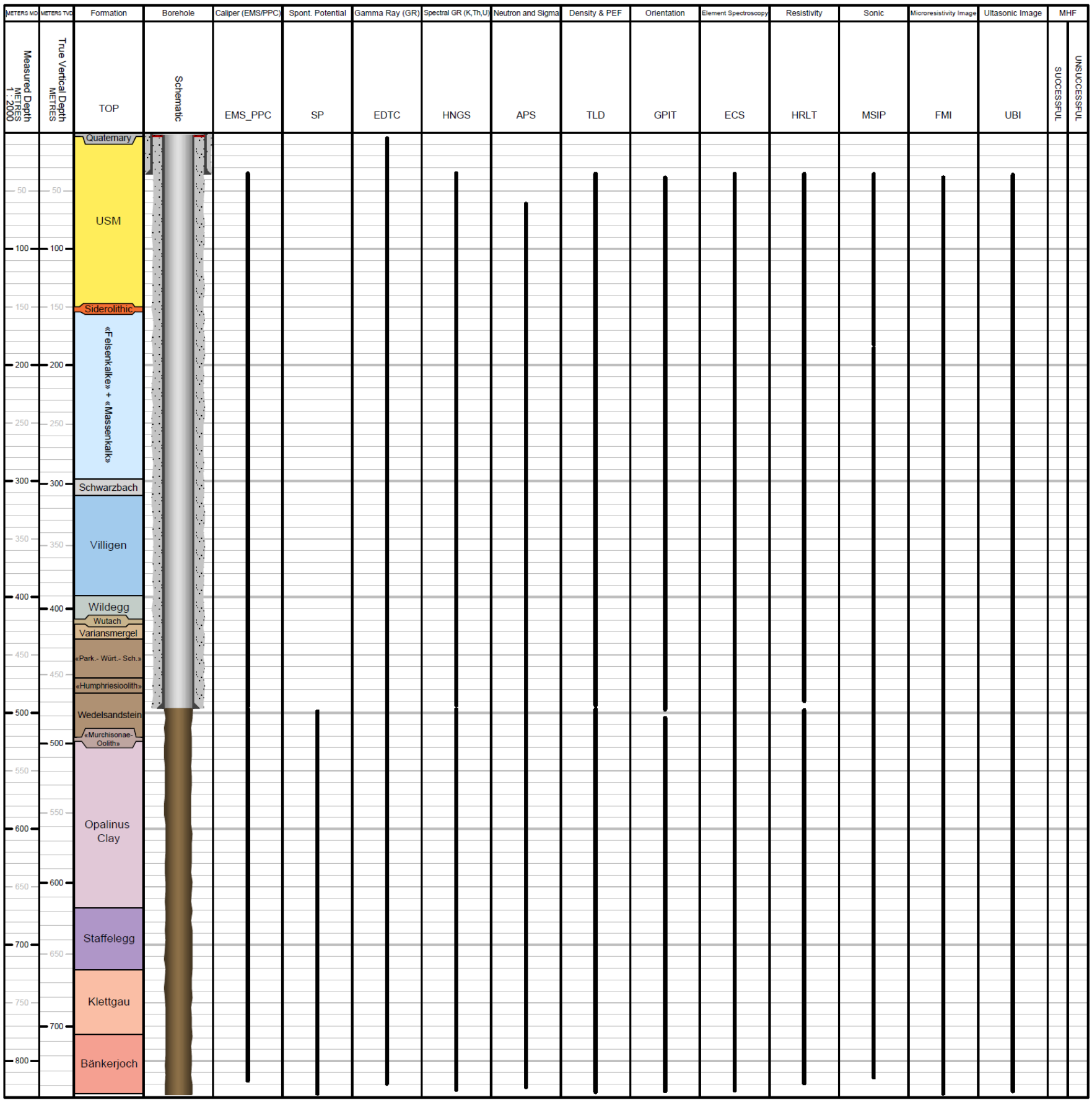

Fig. 2-1: Petrophysical log and MHF testing coverage at RHE1-1 (scale of 1:2'000)

Tab. 2-2: Logging and testing sequence of events (only PL and MHF)

Phase / Section	**Run**	**Operation**	**Logging date**	**Contractor**	**Logging interval** [m MD]	**Logging suite** (see list of abbreviations, Tab. 2-3)	**Measurements**																**Remarks**
							Gamma ray	**Resistivity**	**Microresistivity**	**Density**	**Sonic**	**Neutron hydrogen index**	**Sigma capture cross-section**	**Photoelectric factor**	**Spontaneous potential**	**Borehole imaging**	**Caliper**	**Spectral gamma ray**	**Elemental spectroscopy**	**Inclinometer**	**Temperature**	**MHF**	
I	1.1.1	PL	22. – 23.07.2021	SLB	20.00 to 494.70	FMI-PPC-EMS-EDTC-LEH.QT	×									×	×			×	×		Several attempts were required to reach TD; borehole was undergauge at 456 m and 472 m MD (down to ca. 7"); large amounts of debris were found behind the FMI calipers when rigging down
	1.1.2		23.07.2021	SLB	25.00 to 493.30	UBI-GPIT-EDTC-LEH.QT	×									×				×			The main pass was split into two passes because the sub stopped rotating due to debris
	1.1.3		23.07.2021	SLB	25.00 to 496.00	BNS-PPC-MSIP-PPC-GPIT-EDTC-LEH.QT	×				×						×			×			A bottom nose (BNS) was added to the tool string due to conveyance problems encountered in the first two runs; the BNS improved conveyance greatly and was therefore added to the remaining runs in this section

Tab. 2-2: continued

Phase / Section	Run	Operation	Logging date	Contractor	Logging interval [m MD]	Logging suite (see list of abbreviations, Tab. 2-3)	Measurements																Remarks
							Gamma ray	Resistivity	Microresistivity	Density	Sonic	Neutron hydrogen index	Signa capture cross-section	Photoelectric factor	Spontaneous potential	Borehole imaging	Caliper	Spectral gamma ray	Elemental spectroscopy	Inclinometer	Temperature	MHF	
I	1.1.4	PL	23. – 24.07.2021	SLB	25.00 to 495.50	BNS-TLD-MCFL-EDTC-LEH.QT	×		×	×				×									The caliper was not fully opened until 475.00 m MD
	1.1.5		24.07.2021	SLB	25.00 to 494.80	BNS-APS-EMS-EDTC-LEH.QT	×					×	×				×				×		The minitron automatically shut down at 60 m MD for safety reasons associated with the radioactive source; therefore no APS data were acquired above this depth
	1.1.6		24.07.2021	SLB	25.00 to 495.30	BNS-ECS-EDTC-LEH.QT	×												×				
	1.1.7		24.07.2021	SLB	25.00 to 493.80	BNS-HNGS-EDTC-LEH.QT	×											×					
	1.1.8		25.07.2021	SLB	25.00 to 490.65	BNS-HRLT-PPC-EMS-EDTC-LEH.QT	×	×									×				×		SP could not be acquired in this section because the tool was not compatible with the logging truck
II	2.2.1	PL	18.08.2021	SLB	400.00 to 828.14	FMI-PPC-EMS-EDTC-LEH.QT	×									×	×			×	×		
	2.2.2		19.08.2021	SLB	480.00 to 826.46	UBI-GPIT-EDTC-LEH.QT	×									×				×			

Tab. 2-2: continued

Phase / Section	**Run**	**Operation**	**Logging date**	**Contractor**	**Logging interval** [m MD]	**Logging suite** (see list of abbreviations, Tab. 2-3)	**Measurements**																**Remarks**
							Gamma ray	**Resistivity**	**Microresistivity**	**Density**	**Sonic**	**Neutron hydrogen index**	**Signa capture cross-section**	**Photoelectric factor**	**Spontaneous potential**	**Borehole imaging**	**Caliper**	**Spectral gamma ray**	**Elemental spectroscopy**	**Inclinometer**	**Temperature**	**MHF**	
II (continued)	2.2.3	PL	19.08.2021	SLB	5.00 to 500.00	GPIT-PPC-MSIP-PPC-EDTC-LEH.QT (Cased hole)	×				×						×			×			Open hole and cased hole logging were originally planned in one run however, only the cement bond logs (CBL) were acquired because the tool string was unable to pass below 732 m MD
	2.2.4		20.08.2021	SLB	470.00 to 825.61	Roller-GPIT-PPC-MSIP-PPC-EDTC-LEH.QT (Open hole)	×				×						×			×			An impact selector roller was added to the tool string to help pass an obstruction at 732 m MD; as the roller worked well it was added to the remaining open hole runs in this section
	2.2.5		20.08.2021	SLB	480.00 to 827.30	Roller-TLD-MCFL-EDTC-LEH.QT	×		×	×				×									
	2.2.6		20.08.2021	SLB	480.00 to 823.60	Roller-APS-EMS-EDTC-LEH.QT	×					×	×				×				×		
	2.2.7		20.08.2021	SLB	480.00 to 825.21	Roller-ECS-EDTC-LEH.QT	×												×				
	2.2.8		21.08.2021	SLB	480.00 to 825.21	Roller-HNGS-EDTC-LEH.QT	×											×					
	2.2.9		21.08.2021	SLB	480.00 to 820.70	Roller-SP-EMS-HRLT-EDTC-LEH.QT	×	×							×		×				×		

Tab. 2-3: Tool mnemonics and measurement details

Logging tool	**Wireline contractor**	**Mnemonic**	**Principal measurement**
APS	SLB	Accelerator porosity sonde	Epithermal and thermal neutrons, sigma capture cross-section of thermal neutrons
BNS	SLB	Bottom nose	Hole finder
ECS	SLB	Elemental capture spectroscopy sonde	Measurement of the relative dry weight element concentration (e.g. Si, Ca, Fe, S, Ti, Gd, Cl and H) and mineralogical model
EDTC	SLB	Enhanced digital telemetry cartridge	Gamma ray measurement of the total natural radioactivity
EMS	SLB	Environmental measurement sonde	6-arm caliper, temperature and mud resistivity
FMI	SLB	Fullbore formation microimager	Microresistivity imaging tool (pad contact)
GPIT	SLB	General purpose inclinometry tool	Orientation/inclination of the borehole
HNGS	SLB	Hostile natural gamma ray sonde	Spectral gamma ray measurements of natural radioactivity (potassium, thorium, uranium)
HRLT	SLB	High resolution laterolog array tool	Laterolog resistivity measurement at different depths of investigation
LEH.QT	SLB	Logging equipment head with tension	Head tension
MCFL	SLB	Microcylindrically focused log	Measures the invaded zone resistivity (RXO)
MSIP	SLB	Modular sonic imaging platform (sonic scanner)	Compressional, shear and Stoneley wave slowness measurements (monopole and dipole sources); cement bond log
PPC	SLB	Power positioning calipers	4-arm caliper that gives dual axis borehole measurements
SP	SLB	Spontaneous potential	Measurement of electrical potential difference between the borehole and the surface
TLD	SLB	Three-detector lithology density	Bulk density and photoelectric absorption factor measurement
UBI	SLB	Ultrasonic borehole imager	High-resolution acoustic (ultrasonic) images of the borehole

3 Petrophysical Logging (PL)

3.1 Petrophysical logging tools and measurements

Below the main petrophysical measurements acquired, and the downhole logging tools deployed are summarised. A detailed description of how the different tools measure the respective parameters and the underlying physics behind these measurements is not the focus of this report. Borehole imaging tools are described in Chapter 4.

- **Borehole deviation / orientation** (GPIT – General Purpose Inclinometry Tool). The GPIT outputs inclinometer measurements. Tool orientation is defined by three parameters: tool deviation, tool azimuth and relative bearing. Borehole trajectory is calculated from the inclinometer measurements. Inclinometer measurements serve to reference the oriented logs (e.g. borehole imagery and sonic dipole logs).
- **Caliper log** (EMS/PPC – Environmental Measurement Sonde/Powered Positioning Caliper). The caliper log uses several coupled pairs of mechanical arms (2 pairs with PPC, 3 pairs with EMS) to continuously measure the borehole shape in different orientations.
- **Density** (TLD – Three-detector Lithology Density). TLD is an induced radiation tool that measures the bulk density of the formation and the photoelectric factor (PEF). It uses a radioactive source to emit gamma photons into the formation. The gamma rays undergo Compton scattering by interacting with the atomic electrons in the formation. Compton scattering reduces the energy of the gamma rays in a stepwise manner and scatters the gamma rays in all directions. When the energy of the gamma rays is less than 0.5 MeV, they can undergo photoelectric absorption by interacting with the electrons. The flux of gamma rays that reach each of the detectors of the TLD is therefore attenuated by the formation, and the amount of attenuation is dependent upon the density of electrons in the formation, which is related to its bulk density. The bulk density of a rock is the sum of the minerals (solids) and fluids volumes (porosity) times their densities. Hence, the formation density tool is key for the determination of porosity, the detection of low-density fluids (gasses) in the pores and mineralogical identification. In addition, the TLD provides the **photoelectric absorption index** (photoelectric factor – PEF), which represents the probability that a gamma photon will be photoelectrically absorbed per electron of the atoms that compose the material. The PEF characterises the mineralogy. The TLD tool is housed in the High-Resolution Mechanical Sonde that also includes the Micro-Cylindrically Focused Log (MCFL) sonde, that measures the **microresistivity** or alternatively, the resistivity very close to the borehole wall (RXOZ). The bulk density was integrated over depth, to provide the overburden pressure or vertical stress (Sv).
- **Element Spectroscopy** (ECS – Elemental Capture Spectroscopy). The ECS is also an induced radiation tool with a radioactive neutron source. The ECS measures the concentration of a series of elements in the formation (Si, Ca, Fe, S, Ti, Gd, Cl, H) by analysing the gamma ray spectrum of back scattered gamma rays. Special processing techniques allow under certain circumstances the measurement of supplementary elements such as Al, Mg, K and Na. The element spectroscopy measurements are provided in dry weight concentrations. SLB uses an algorithm in the field to derive a model of dry weight fractions of preset minerals from the dry weight element concentrations: clay, clastics (quartz – feldspar – mica, QFM), carbonates, anhydrite / gypsum, salt / evaporite, pyrite, siderite and coal. Advanced models can discriminate limestone and dolomite from carbonates, as well to provide a more quantitative clay measurement. It is important to note that mineralogy model processing is qualitative and should be viewed as an indicator of lithology and not used in any quantitative analysis. Quantitative analysis of the ECS dry weight elements needs to be calibrated against core data.

Dossier X details stochastic processing and interpretation of the ECS dry weight proportions, combined with conventional petrophysical log response, to generate a quantified lithology determination.

- **Gamma Ray** (GR, from the EDTC – Enhanced Digital Telemetry Cartridge). This log measures the total naturally occurring gamma ray radioactivity in the formation rocks (potassium, thorium and uranium are the most common radioactive elements in Earth's crust), which can be used to determine the volume of clay minerals (that contains those elements). The GR log is not valid for clay determination if other minerals contain those elements in significant amounts (e.g. potassic feldspars, organic matter, phosphates). The GR is run with all logging runs because it is used for depth correlation between runs, thanks to its excellent vertical resolution and character. Note this is not to be confused with the Spectral Gamma Ray which is a different tool detailed further below.
- **Neutron Hydrogen Index, commonly named Neutron** (NHI, from the APS – Accelerator Porosity Sonde). A particular accelerator called a Minitron generates high energy neutrons (14 MeV) that are emitted into the formation. Elastic collisions with the atom nuclei slow down the neutrons, a process that is more efficient with nuclei whose mass is close to that of neutron, i.e., hydrogen (the lightest element). Five detectors count the neutrons back from the formation at different distances from the Minitron, allowing for an environmental compensation of the signal. The received signal is mostly (but not only, for example the chlorine atoms bring a significant contribution) dependent on the hydrogen concentration in the formation, hence the Hydrogen Index (HI) measurement: the larger the count, the lower the HI and its uncertainty. The APS tool can measure both an epithermal HI (APLC curve) and a thermal HI (FPLC). The hydrogen content in rocks is mostly in the fluids contained within, generally water or hydrocarbons, which have a HI close to 1 v/v. Nevertheless, some fluids like gas and high salinity brines have a HI lower than 1 v/v and must be corrected for when interpreting the results. In addition, many hydrated minerals are encountered in sedimentary or crystalline rocks, e.g. clay minerals, gypsum, iron-hydroxides, coals, zeolites, micas and amphiboles. The NHI is commonly used to quantify the fluid volume (porosity) and as a lithological indicator (clay content, hydrogen-rich minerals), mostly in combination with the bulk density measurement.
- **Resistivity** (HRLT – High Resolution Laterolog array Tool). The HRLT measures electrical resistivities at different depths of investigation in the formation. When drilling mud filtrate invades the formation and it has a salinity that contrasts with that of the formation fluids (the chlorine ion Cl^- changes significantly the resistivity of a medium), the resistivities provide an invasion profile. Processing allows the extrapolation of the resistivity measurements far into the formation providing the true formation resistivity, as well as close to the tool providing the microresistivity or resistivity close to the borehole wall. Resistivity is used to interpret the saturation in water or hydrocarbons in pore spaces and for mineralogical identification (e.g. carbonates, clays, salt).
- **Sigma Formation Capture Cross-Section** (SIGF, from APS). In addition to the HI, the APS also measures the sigma formation capture cross-section (SIGF), that is defined as the relative ability of a material to "capture" or absorb free thermal neutrons. SIGF values vary widely with elements, and it can be used to determine the mineralogy and formation fluid contents.
- **Sonic** (MSIP – Modular Sonic Imaging Platform, also named Sonic Scanner). The MSIP measures how fast compressional and shear waves travel in the formation. A pulse sound is emitted from several tool transmitters in all directions. Tool receivers record the waves after they have travelled through a known path in the formation to the borehole wall. Waves travel at different velocities in the drilling fluid (between the tool and the borehole wall) and in the formation. Subtracting the travel time recorded by the near transmitter-receiver pairs from the

travel time recorded by far transmitter-receiver pairs provides the travel time spent in the formation only and thus discards the wave propagation in the fluid. Travel times are converted to wave slowness logs (inverse of velocity) based on the tool geometry. Compressional and shear wave slowness are used to interpret porosity, aid in mineralogy determination, for geomechanical and rock strength properties and they serve as calibration for seismic surveys. Other wave propagation such as flexural waves can be used to analyse the acoustic shear anisotropy properties of the formation. The MSIP log products require processing of the raw data to detect the different wave arrivals and transform the multiple transmitter-receiver recordings into unique slowness logs. Field processing products are basic and advanced processing products, such as the anisotropy analysis can be requested at a later stage.

- **Spectral Gamma Ray** (SGR, from the HNGS – Hostile Natural Gamma Ray Sonde). In addition to the total gamma ray, the HNGS measures the energy spectrum of the formation gamma rays. As the three main radioactive elements (potassium, thorium and uranium) are characterised by a different gamma energy, the tool can quantify those elements' content. Those concentrations can be used to quantify potassium-, uranium- or thorium-rich minerals (e.g. different clay minerals, potassic feldspars, organic matter, phosphates). The HSGR log is the sum of potassium, thorium and uranium gamma ray contributions to the total spectral gamma ray. Note that the total gamma ray from the GR and SGR tools are not necessarily quantitatively equivalent because these tools use different detectors, technologies, tool housing and calibrations. The HCGR log is the result of the HSGR log without the uranium contribution. The shading from HCGR to HSGR in log plots helps identify zones that may contain uranium-bearing organic matter and phosphates.
- **Spontaneous Potential** (SP). The SP log is a continuous measurement of the electric potential difference between an electrode in the SP tool and a surface electrode. Adjacent to shales, SP readings usually define a straight line known as the shale baseline. Next to permeable formations, the curve departs from the shale baseline; in thick permeable beds, these excursions reach a constant departure from the shale baseline, defining the "sand line". The deflection may be either to the left (negative) or to the right (positive), depending on the relative salinities of the formation water and the mud filtrate. If the formation water salinity is greater than the mud filtrate salinity (the more common case), the deflection is to the left. The movement of ions, essential to develop an SP, is possible only in rocks with some permeability, a small fraction of a millidarcy is sufficient. There is no direct relationship between the magnitude of the SP deflection and the formation's permeability or porosity.
- **Temperature** (TMP). The temperature log is acquired with the EMS tool that includes a temperature sensor. It is a measurement of the temperature in the borehole environment; thus, it is largely influenced by the temperature of mud. Since the temperature is affected by material outside the casing, a temperature log is sensitive to not only the borehole but also the formation and the casing – formation annulus. Mud temperature is generally less than that of fluids in the formation, but the temperature of the static mud is assumed to converge to the formation temperature after an infinite time. In practice, temperature logs are acquired several times after the last mud circulation, and the formation temperature is modelled based on the observed trend of temperature vs. time at each depth. On one hand, the temperature log is interpreted by looking for larger scale anomalies, or departures, from a reference gradient. This can give indications for permeable zones with fluid flow or for flow barriers hindering cross formational flow. On the other hand, localised smaller scale anomalies may correspond to the entry of borehole mud in the formation or fluid flow from the formation to the borehole. The temperature log should be interpreted together with structural geology, hydrogeology, and the other logs (e.g. images, resistivity logs).

3.2 Log data quality

3.2.1 Quality control procedures

Quality control (QC) of log data is important to guarantee their accuracy, repeatability, traceability, relevance, completeness, sufficiency, interpretability, clarity and accessibility. The generic QC procedures that were followed for each log dataset are presented as follows:

1. Digital data in .dlis format are loaded into a petrophysics software (Paradigm – Geolog) and checked for completeness (Are principal log channels, parameters and constants given?) and accessibility (Do the data load correctly when imported? Is the depth sampling rate steady and valid?).
2. Sufficient data: Do the first and last readings correspond to the interval of logs laid-out in the work programme?
3. Depth match is checked: main pass (or downlog pass if first run in hole) versus reference run, repeat pass(es) versus reference run. GR log of the EDTC tool is always used for correlation because it has excellent vertical resolution and sufficient character. Schlumberger depth matches data in the field, but sometimes additional depth-matching is required during QC. Such depth shifts are recorded in App. A8 – Table of post-acquisition depth shifts.
4. Are the calipers well calibrated? This is checked by comparing caliper measurements against the nominal inner diameter of the casing.
5. Borehole shape is checked: Are there washouts? Is the borehole on gauge? Undergauge? Ovalised? Are there breakouts? Hole restrictions? If the borehole shape is not gauge, the log quality can be degraded.
6. Cable tension is checked: does the cable tension show any overpulls or stick and pull events? These events can cause a locally discontinuous depth log measurement and alter the tool positioning which impacts the log quality. The tension log is also used to check that the logger depth is consistent with the tension pick-up.
7. Graphic files (log plots) are checked for completeness, consistency and accuracy. In particular, the following sections of the graphic files are checked:
   - 7.1 Header: e.g. logging date, run number, mud parameters
   - 7.2 Borehole sketch and size / casing record: hole bit sizes and depths, casing sizes, weight and depth
   - 7.3 Borehole fluids: accuracy of mud physical parameters
   - 7.4 Remarks and equipment summary: serial numbers of equipment, completeness and accuracy of remarks
   - 7.5 Depth control parameters: right depth control procedure and log of reference
   - 7.6 Summary of run passes: top and bottom of pass, automatic bulk shift applied
   - 7.7 Log (content and display): mnemonics, description, unit, scale, colour and label of logs; display of logs, log quality control (LQC) or data copy indicator curves provided (if applicable)
   - 7.8 Channel processing parameters, tool control parameters: corrections or offsets applied to measurements, modes of acquisition etc.
   - 7.9 Accelerometer and magnetometer crossplots provided (if applicable)
   - 7.10 Calibration reports: validity of master calibration and before calibration (if applicable), all calibrations within tolerances

8. Data repeatability for main vs. repeat passes (or downlog pass if applicable) is checked for a selection of important logs.
9. Were required, environmental corrections applied with the correct parameter values (e.g. mud salinity, mud weight, drill bit size, tool standoff, pressure / temperature).
10. Were processing parameters correctly applied (e.g. ECS minerals model options, MSIP time windows, APS lithology conversions)?
11. Data consistency is checked, including a comparison with logs from other runs via log plot and crossplots and the description of the cuttings for lithology. Are logs representative of expected lithologies and do they respond consistently?
12. Are orientation, accelerometer and magnetometer data accurate? This is essential for all data-sets that need to be oriented (e.g. borehole imagery [FMI/UBI], dipole sonic).
13. Mud resistivity and borehole temperature are checked for repeatability and checked against collected mud samples and thermometers in the logging head.
14. Quality of automatic picking on processing products (if applicable), e.g. compressional and shear wave slowness picking on semblance projections for sonic logs.

3.2.2 Bad-hole flags

To complete the data QC process, bad-hole flags were created to highlight zones where the log quality was degraded by 'bad-hole' conditions and should be viewed with caution. The methodology is presented in Tab. 3-1 and explained in detail in Appendix A7 – Badhole & unfit data flags.

Bad hole is a common issue with logging. It means that the borehole conditions are inadequate for obtaining optimum quality petrophysical logs that truly represent the formation that is being logged. The tools that either measure petrophysical properties in a space volume or must be in continuous contact with the borehole wall during logging (eccentered tools) are the most affected by bad hole. Washouts and rugose hole are the most common features that degrade the quality of the logs resulting for example in the underestimation of density and overestimation of sonic slowness.

Tab. 3-1: Bad-hole flag methodology

Bad-hole logic	**Logs used**	**Cutoff/method**
Overgauge flag	Caliper	Borehole diameter is greater than 115% of nominal drill bit size
Rugosity flag	Density correction (HDRA), acquired with TLD	The density correction log is calculated from the difference between the short- and long-spaced density measurements, an indicator of borehole rugosity and density quality. Density is not reliable when HDRA > 0.025 g/cm^3
Neutron standoff	Neutron standoff (STOF), acquired with APS	Neutron tool should be flushed with borehole wall or should have pre-determined physical standoff. If unintentional standoff, STOF > 0.35", bad hole is flagged
Density-neutron flag	Density (RHOZ) and neutron (APLC)	Systematic identification of outliers in density-neutron crossplot and comparison with analogue data from adjacent boreholes

3.3 Composite log generation

The objective of the composite log dataset is to provide a traceable quality-controlled, edited, corrected and merged dataset for all petrophysical logging data recorded across the entire length of the borehole. Petrophysical tools acquire many logs that are not directly related to petrophysical properties but are needed to control that the tool sensors worked well (e.g. mechanical or electronics status of the sensors). In addition, some logs are acquired several times in a section (e.g. GR, Temperature). Ad Terra selects a collection of the most relevant logs for formation evaluation, correlation and calibration with core or seismic data. Some 112 representative logs are thus extracted for each borehole section. These logs are:

1. quality controlled (procedures in Section 3.2.1)
2. edited e.g. to keep data points that are true responses of the borehole and formation environment
3. further corrected for the borehole environment or artefacts
4. merged into composite logs that cover the entire or most of the borehole
5. The generated composite log dataset is generated and delivered in standard digital (LAS – Log ASCII Standard) and graphic (PDF log plot) format.

A more detailed procedure for the generation of the composite log is detailed in the next subchapter. In addition, a complete report in Excel format is provided (see Appendix A) which details all relevant information about the logs and the acquisition runs. Appendix A5 – Composite log generation worksheet specifically details how the composite log dataset was generated through merging techniques.

3.3.1 Generic process

The following steps were conducted to generate the composite log dataset:

1. A bit size log was generated according to the borehole design at the time of logging (see Appendix A2 – Borehole design).
2. Logs were depth-shifted as required (see Appendix A8 – Post-acquisition depth shifts).
3. First and last readings were edited to remove values acquired before the tool sensors started reading the borehole (e.g. constant values just before/after the sensor is switched off/on) and/or before the tools started to move upward (e.g. stationary measurements close to total depth). Log readings were further edited if they did not read the borehole formation environment, e.g. logs can be impacted by the nearby casing shoe and cement, become decentralised when there are changes in the borehole diameter, or sediment infills at bottom of the borehole.
4. All logs that were not valid in cased hole were discarded. For the RHE1-1 composite log dataset, this included all logs except for the total gamma ray log (ECGR_EDTC) from the EDTC and borehole temperature (TMP) from the EMS.
5. Bad-hole flags were created based on advanced log analysis to highlight zones where the log quality was affected by bad-hole conditions.
6. Total gamma ray log (ECGR_EDTC) was corrected for the radioactive potassium silicate in the drilling mud using the borehole potassium corrected total spectral gamma ray log (HSGR) for calibration. It was further normalised to account for attenuated readings in cased hole intervals according to standard practice. The corrected gamma ray log was then renamed GR_KCOR.
7. Poor quality sonic slowness data (DTCO, DTSM) caused by imprecise automatic picking were removed and interpolated where applicable.
8. The edited and corrected logs from each section were merged. Merging points were chosen carefully to optimise log coverage and composite log consistency. See Appendix A5 – Composite log generation.
9. Standardised log names, units and descriptions were used.
10. Logs acquired at higher resolution (e.g. RHO8, PEF8 have sample rates 0.0508 m – ⅙ ft) were resampled to the standard rate of 0.1524 m (½ ft), because the digital LAS format cannot support mixed sample rates.
11. Final log plots at a scale of 1:200 m MD, 1:1'000 m MD and 1:2000 m MD were produced in PDF graphic file format along with digital data in LAS format.

The composite Excel report and log plots at a scale of 1:200 m and 1:1'000 m MD and TVD can be found in Appendix A, Appendix B and Appendix C, respectively. Tab. 3-2 lists and describes all the log curves / channels that are provided in the composite log set.

Tab. 3-2: Composite log LAS channel listing

Curve / channel	**Units**	**Description**
DEPTH	M	
APLC	V/V	Near/array Corrected Limestone Porosity (Epithermal HI)
BS	IN	Bit Size
DEVI	DEG	Borehole deviation
DTCO	US/F	Delta-T Compressional
DTSM	US/F	Delta-T Shear
DWAL_ALKNA	W/W	Dry Weight Fraction Pseudo Aluminium (SpectroLith ALKNA Model)
DWAL_MGWALK	W/W	Dry Weight Fraction Pseudo Aluminium (SpectroLith MWGALK Model)
DWAL_WALK2	W/W	Dry Weight Fraction Pseudo Aluminium (SpectroLith WALK2 Model)
DWCA_ALKNA	W/W	Dry Weight Fraction Calcium (SpectroLith ALKNA Model)
DWCA_MGWALK	W/W	Dry Weight Fraction Calcium (SpectroLith MGWALK Model)
DWCA_WALK2	W/W	Dry Weight Fraction Calcium (SpectroLith WALK2 Model)
DWCL_ALKNA	W/W	Dry Weight Fraction Chlorine Associated with Salt (SpectroLith ALKNA Model)
DWCL_MGWALK	W/W	Dry Weight Fraction Chlorine Associated with Salt (SpectroLith MGWALK Model)
DWCL_WALK2	W/W	Dry Weight Fraction Chlorine Associated with Salt (SpectroLith WALK2 Model)
DWFE_ALKNA	W/W	Dry Weight Fraction Iron + 0.14 Aluminium (SpectroLith ALKNA Model)
DWFE_MGWALK	W/W	Dry Weight Fraction Iron + 0.14 Aluminum (SpectroLith MGWALK Model)
DWFE_WALK2	W/W	Dry Weight Fraction Iron + 0.14 Aluminium (SpectroLith WALK2 Model)
DWGD_ALKNA	PPM	Dry Weight Fraction Gadolinium (SpectroLith ALKNA Model)
DWGD_MGWALK	PPM	Dry Weight Fraction Gadolinium (SpectroLith MGWALK Model)
DWGD_WALK2	PPM	Dry Weight Fraction Gadolinium (SpectroLith WALK2 Model)
DWHY_ALKNA	W/W	Dry Weight Fraction Hydrogen Associated with Coal (SpectroLith ALKNA Model)
DWHY_MGWALK	W/W	Dry Weight Fraction Hydrogen Associated with Coal (SpectroLith MGWALK Model)
DWHY_WALK2	W/W	Dry Weight Fraction Hydrogen Associated with Coal (SpectroLith WALK2 Model)
DWK_ALKNA	W/W	Dry Weight Fraction Potassium (SpectroLith ALKNA Model)
DWK_MGWALK	W/W	Dry Weight Fraction Potassium (SpectroLith MGWALK Model)
DWMG_MGWALK	W/W	Dry Weight Fraction Magnesium (SpectroLith MGWALK Model)
DWSI_ALKNA	W/W	Dry Weight Fraction Silicon (SpectroLith ALKNA Model)
DWSI_MGWALK	W/W	Dry Weight Fraction Silicon (SpectroLith MGWALK Model)
DWSI_WALK2	W/W	Dry Weight Fraction Silicon (SpectroLith WALK2 Model)

Tab. 3-2: continued

Curve / channel	**Units**	**Description**
DWSU_ALKNA	W/W	Dry Weight Fraction Sulphur (SpectroLith ALKNA Model)
DWSU_MGWALK	W/W	Dry Weight Fraction Sulphur (SpectroLith MGWALK Model)
DWSU_WALK2	W/W	Dry Weight Fraction Sulphur (SpectroLith WALK2 Model)
DWTI_ALKNA	W/W	Dry Weight Fraction Titanium (SpectroLith ALKNA Model)
DWTI_MGWALK	W/W	Dry Weight Fraction Titanium (SpectroLith MGWALK Model)
DWTI_WALK2	W/W	Dry Weight Fraction Titanium (SpectroLith WALK2 Model)
FLAG_BADHOLE_OVERGAUGE		Overgauge Borehole Bad-Hole Flag
FLAG_BADHOLE_RUGO		Rugose Borehole Bad-Hole Flag
FLAG_BADHOLE_STOF		Neutron Porosity Standoff Bad-Hole Flag
FLAG_UNFIT_ND		Flag that indicates unfit neutron-density data for deterministic log evaluation
FPLC	V/V	Near/Far Corrected Limestone Porosity (Thermal HI)
GR_KCOR	GAPI	Total natural radioactivity corrected for the borehole potassium (EDTC)
HAZI	DEG	Borehole azimuth
HCGR	GAPI	HNGS Computed Gamma Ray
HDAR	IN	Hole Diameter from Area
HDRA	G/C3	Density Standoff Correction
HFK	%	HNGS Formation Potassium Concentration
HSGR	GAPI	HNGS Standard Gamma-Ray
HTHO	PPM	HNGS Formation Thorium Concentration
HURA	PPM	HNGS Formation Uranium Concentration
PEF8	B/E	High Resolution Formation Photoelectric Factor
PEFZ	B/E	Standard Resolution Formation Photoelectric Factor
RD1	IN	Radius 1
RD2	IN	Radius 2
RD3	IN	Radius 3
RD4	IN	Radius 4
RD5	IN	Radius 5
RD6	IN	Radius 6
RHGE_ALKNA*	G/C3	Matrix Density from Elemental Concentrations (SpectroLith ALKNA Model)
RHGE_MGWALK*	G/C3	Matrix Density from Elemental Concentrations (SpectroLith MGWALK Model)
RHGE_WALK2*	G/C3	Matrix Density from Elemental Concentrations (SpectroLith WALK2 Model)
RHO8	G/C3	High Resolution Formation Density
RHOZ	G/C3	Standard Resolution Formation Density
RLA0	OHMM	Apparent Resistivity from Computed Focusing Mode 0
RLA1	OHMM	Apparent Resistivity from Computed Focusing Mode 1

Tab. 3-2: continued

Curve / channel	**Units**	**Description**
RLA2	OHMM	Apparent Resistivity from Computed Focusing Mode 2
RLA3	OHMM	Apparent Resistivity from Computed Focusing Mode 3
RLA4	OHMM	Apparent Resistivity from Computed Focusing Mode 4
RLA5	OHMM	Apparent Resistivity from Computed Focusing Mode 5
RT_HRLT	OHMM	HRLT True Formation Resistivity
RXO8	OHMM	Invaded Formation Resistivity filtered at 8 inches
RXOZ	OHMM	Invaded Formation Resistivity filtered at 18 inches
RXO_HRLT	OHMM	HRLT Invaded Zone Resistivity
SIGF	CU	Formation Capture Cross-Section
SP	MV	Spontaneous Potential
STOF	IN	Effective Standoff in Limestone
STPC	V/V	Corrected Standoff Porosity
SV	MPa	Overburden vertical stress (Sv)
TMP	DEGC	Mud Temperature at the time of logging
U8	B/C3	High Resolution Volumetric Photoelectric Factor
UZ	B/C3	Volumetric Photoelectric Factor
WANH_ALKNA *	W/W	Dry Weight Fraction Anhydrite / Gypsum (SpectroLith ALKNA Model)
WANH_MGWALK *	W/W	Dry Weight Fraction Anhydrite/Gypsum (SpectroLith MGWALK Model)
WANH_WALK2 *	W/W	Dry Weight Fraction Anhydrite / Gypsum (SpectroLith WALK2 Model)
WCAR_ALKNA *	W/W	Dry Weight Fraction Carbonate (SpectroLith ALKNA Model)
WCAR_MGWALK *	W/W	Dry Weight Fraction Carbonate (SpectroLith MGWALK Model)
WCAR_WALK2 *	W/W	Dry Weight Fraction Carbonate (SpectroLith WALK2 Model)
WCLA_ALKNA *	W/W	Dry Weight Fraction Clay (SpectroLith ALKNA Model)
WCLA_MGWALK *	W/W	Dry Weight Fraction Clay (SpectroLith MGWALK Model)
WCLA_WALK2 *	W/W	Dry Weight Fraction Clay (SpectroLith WALK2 Model)
WCLC_MGWALK *	W/W	Dry Weight Fraction Calcite (SpectroLith MGWALK Model)
WCOA_ALKNA *	W/W	Dry Weight Fraction Coal (SpectroLith ALKNA Model)
WCOA_MGWALK *	W/W	Dry Weight Fraction Coal (SpectroLith MGWALK Model)
WCOA_WALK2 *	W/W	Dry Weight Fraction Coal (SpectroLith WALK2 Model)
WDOL_MGWALK *	W/W	Dry Weight Fraction Dolomite (SpectroLith MGWALK Model)
WEVA_ALKNA *	W/W	Dry Weight Fraction Salt (SpectroLith ALKNA Model)
WEVA_WALK2 *	W/W	Dry Weight Fraction Salt (SpectroLith WALK2 Model)
WPYR_ALKNA *	W/W	Dry Weight Fraction Pyrite (SpectroLith ALKNA Model)
WPYR_MGWALK *	W/W	Dry Weight Fraction Pyrite (SpectroLith MGWALK Model)
WPYR_WALK2 *	W/W	Dry Weight Fraction Pyrite (SpectroLith WALK2 Model)

Tab. 3-2: continued

Curve / channel	Units	Description
WQFM_ALKNA *	W/W	Dry Weight Fraction Quartz+Feldspar+Mica (QFM) (SpectroLith ALKNA Model)
WQFM_MGWALK *	W/W	Dry Weight Fraction Quartz+Feldspar+Mica (QFM) (SpectroLith MGWALK Model)
WQFM_WALK2 *	W/W	Dry Weight Fraction Quartz+Feldspar+Mica (QFM) (SpectroLith WALK2 Model)
WSID_ALKNA *	W/W	Dry Weight Fraction Siderite (SpectroLith ALKNA Model)
WSID_MGWALK *	W/W	Dry Weight Fraction Siderite (SpectroLith MGWALK Model)
WSID_WALK2 *	W/W	Dry Weight Fraction Siderite (SpectroLith WALK2 Model)

* Qualitative data should only be used as a lithology indicator.

3.3.2 Gaps in log coverage

Optimising the petrophysical log and MHF testing coverage was an objective of the logging and testing campaigns, in particular for the potential Opalinus Clay rock host. Despite best efforts, gaps in log coverage are an inherent limitation in wireline logging operations.

Complete log coverage at changes in drilling section is possible if the acquisition of the lowermost part of the drilling section is repeated later with the acquisition of the uppermost part of the drilling section below. Logs acquired with the same sensor, which overlap over two sections can then be merged providing complete coverage. This is not always possible due to limitations related to tool string geometry, borehole conditions and borehole design. Examples include:

- Cuttings infill the bottom of the hole preventing the tool string from reaching total depth.
- The tool string should not tag the bottom hole with certain fragile tools (e.g. UBI).
- The offset of the sensors relative to the bottom of the tool string.
- The rathole clearance (space between casing shoe and the bottom of the drilled hole) available for logging in the section below is too short. If the casing shoe is too close to the bottom of the section and the lowermost part of the open hole was not logged before casing installation, some log coverage will be lost.
- The rathole available for logging in the section below is first enlarged, and its diameter is different (e.g. 12¼") from that of the cored section below (6⅜"). Abrupt changes in borehole size are not favourable for logging because they are often associated with bad hole and eccentered tools in contact with the borehole wall acquire logs of degraded quality, causing gaps in log coverage.

The above factors were taken into consideration in the design of work programmes. For each logging campaign, project guidelines defined the balance between the optimisation of log coverage (short tool strings, more runs, longer campaign) and saving rig time and associated costs (slightly longer tool strings, less runs, shorter campaign).

For the main drilling sections where petrophysical logs were acquired (Sections I and II), a summary of the meterage of logged data and the percentage of total depth this data represents, is summarised in Tab. 3-3. The Opalinus Clay and bounding formations (Dogger – Lias) were examined in greater detail. Almost complete log coverage was acquired in these formations.

Tab. 3-3: Summary of petrophysical log coverage from drilling Section II to TD

Measurement	**Section I to TD** (35.80 m – 828.00 m MD)		**Opalinus Clay and Bounding Formations (Dogger to Lias)** (419.20 m – 721.50 m MD)	
	Meterage [m]	**Coverage** [%]	**Meterage** [m]	**Coverage** [%]
Caliper	790.19	99.75	300.78	99.50
Borehole orientation	780.44	98.52	295.29	97.68
Total Gamma Ray	814.57	100.00	302.30	100.00
Spontaneous Potential	329.34	41.57	222.85	73.72
Spectral Gamma Ray	786.69	99.30	299.10	98.94
Density	788.31	99.51	299.15	98.96
Photoelectric Factor	788.31	99.51	299.15	98.96
Microresistivity	789.37	99.64	300.62	99.44
Neutron (NHI)	759.88	95.92	300.78	99.50
Sigma Formation Capture Cross-Section	759.88	95.92	300.78	99.50
Resistivity	776.07	97.96	294.53	97.43
Sonic	778.46	98.27	302.30	100.00
Element Spectroscopy	787.45	99.40	300.01	99.24
Ultrasonic Borehole Imagery	780.70	98.55	293.10	96.96
Microresistivity Borehole Imagery	780.20	98.49	293.20	96.99

The depths at which there were gaps in log coverage in the final composite dataset are detailed in Appendix A5 – Composite log generation.

3.4 Petrophysical logging results and description

The main features of the petrophysical logs of the composite dataset are described below by litho-stratigraphic units.

3.4.1 Tertiary: Untere Süsswassermolasse (USM) and Siderolithic (3 m to 154.40 m MD)

The top of the USM was identified at 3 m MD based on the description of the cuttings before installing the conductor pipe. Wireline logs did not measure the horizon. The Tertiary units were drilled destructively, so no core was acquired.

Log responses did not always reflect the borehole lithology well, in particular in the more clay-rich zones, which resulted in less favourable (bad-hole) conditions. While the borehole diameter was generally in gauge, the borehole wall was rugose, which affected the response of tools in contact with the wall (e.g. density, neutron, ECS) as well as the sonic tool.

Logs in the USM and Siderolithic are characterised by the following (Fig. 3-1):

- Zones with good-hole conditions generally show a low to moderately low clay content: intermediate total GR (GR_KCOR: 40 to ca. 81 GAPI) and sigma (SIGF: 13.8 to ca. 21 CU).
- Conversely, zones with bad-hole conditions generally have a higher clay content, as indicated by the high GR_KCOR (higher than ca. 81 GAPI) and SIGF (higher than ca. 21 CU).
- Matrix mineralogy is dominated by quartz or siliciclastics such as potassium feldspars: inverse density-neutron separation displayed in the limestone-compatible scale (shaded yellow in Fig. 3-1), low PEFZ and intermediate to high silicon content (DWSI: 0.15 W/W to 0.35 W/W; pure quartz: 0.467 W/W). In the zones with a higher clay content, the density-neutron separation is normal (shaded brown) despite the siliciclastics, because the log response is also influenced by the clay. It is assumed that radioactive minerals, such as potassium feldspars or micas, are present in the matrix mineralogy based on the GR_KCOR and SIGF readings that are higher than expected for low to moderately low clay content.
- The upper part of the USM from 3 m to 93.00 m MD is richer in siliciclastics, whereas the lower USM from 93.00 m to 149.90 m MD contains more carbonates: higher ECS calcium dry weight fraction readings (DWCA: up to 0.21 W/W).
- Several zones rich in organic matter (such as coal beds) were observed from 50.70 m to 55.90 m MD, at 75.00 m MD, at 80.30 m MD and from 92.00 m to 94.00 m MD: high total GR (up to 503 GAPI) and high uranium content (up to 46.5 ppm).
- The Siderolithic unit is characterised by a high ECS iron dry weight fraction (DWFE: ranging from 0.04 W/W to 0.13 W/W), as well as high thorium (HTHO: up to 23.9 ppm) and sigma (up to 43.9 CU), which suggest the presence of iron-bearing minerals other than clays.

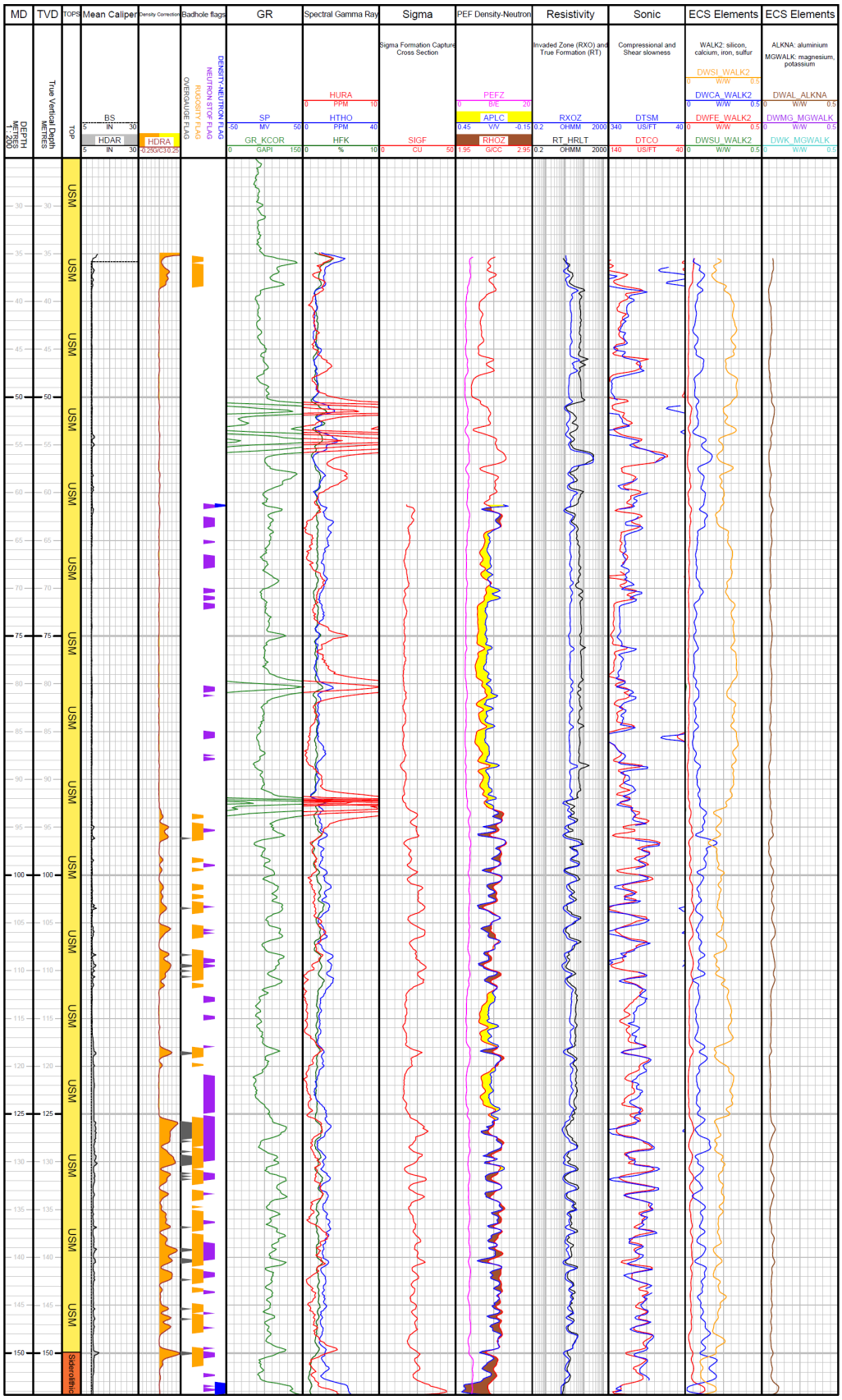

Fig. 3-1: Main logs of the composite dataset in the USM to the Siderolithic Formation

3.4.2 Malm: «Felsenkalke» + «Massenkalk» to Wildegg Formation (154.40 to 419.20 m MD)

The top of the Malm («Felsenkalke» + «Massenkalk») can be identified by a decrease in total GR (GR_KCOR), sigma (SIGF) and sonic (DTCO) logs (Fig. 3-2), when transitioning to the low-clay limestone of the Malm.

Log responses reflected the borehole lithology well, except for some short overgauge and rugose bad-hole zones in the upper «Felsenkalke» + «Massenkalk» and in the lower Wildegg Formation, where the response of most logs was affected, including the neutron, density and sonic logs.

Logs in the Malm units have an overall similar log signature characterised by (Fig. 3-2):

- Generally low clay content: GR (GR_KCOR: 5.7 to 33 GAPI; mean = 17 GAPI), spectral GR (e.g. HTHO: 0.2 ppm to 6.8 ppm thorium; mean = 1.5 ppm) and sigma (SIGF: 6.5 to 20.3 CU; mean = 10.0 CU). Clay content is increased in the Schwarzbach Formation, the Wildegg Formation and from 183.50 m to 191.00 m MD in the «Felsenkalke» + «Massenkalk» (GR_KCOR: 17 to 110 GAPI; mean = 52 GAPI).
- Calcite is the dominant mineral: an almost perfect overlap in the neutron-density limestone-compatible scale (density [RHOZ] and neutron [APLC] readings in pure limestone are 2.71 g/cm^3 and 0.0 v/v, respectively), the calcium dry weight fraction (DWCA) is close to that of pure calcite (0.394 W/W), as is the photoelectric factor (PEFZ) – pure calcite value of 5.1 B/E.
- In the low-clay units (GR_KCOR < 30 GAPI), porosity is low, density is high (rarely lower than 2.60 g/cm^3; mean: 2.67 g/cm^3) and sonic (DTCO) rarely exceeds 71 µs/ft.
- The qualitative classification of clay minerals based on the spectral GR potassium (HFK) and thorium (HTHO) logs is not relevant given the low clay content.

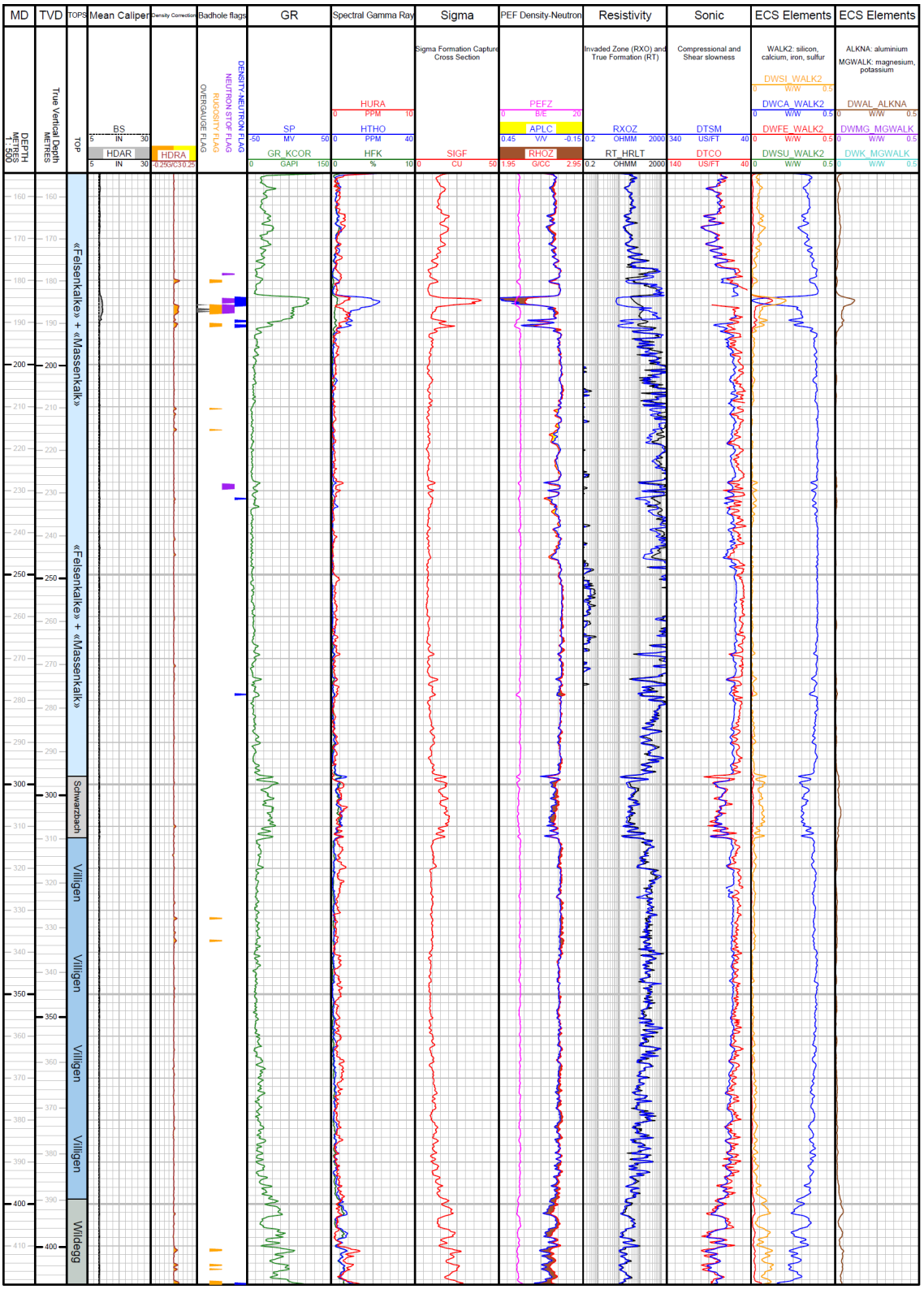

Fig. 3-2: Main logs of the composite dataset in the «Felsenkalke» + «Massenkalk» to the Wildegg Formation

3.4.3 Wutach Formation to «Murchisonae-Oolith Formation» (419.20 m to 524.33 m MD)

The top of the Dogger (Wutach Formation) can be identified by an increase in siderite, iron oxide or hydroxide bearing rock indicators such as the ECS iron dry weight fraction (DWFE), a wide separation in the neutron-density logs (displayed in a limestone-compatible scale) and an increase in PEFZ (Fig. 3-3).

The overall log quality was intermediate to excellent in the units of the «Brauner Dogger». The borehole wall was rugose in parts of the units that were drilled destructively down to 497.00 m MD. Hole conditions were better in the cored interval from 499.10 m MD. Logs have the following attributes:

- Highly variable clay content that is moderately low to intermediate in the «Humphriesioolith Formation» and the Wedelsandstein Formation and moderately high in the Wutach Formation, the Variansmergel Formation, the «Parkinsoni-Württembergica-Schichten» and the «Murchisonae-Oolith Formation». Excluding the zones that contain siderite, iron-oxides or hydroxides (DWFE > 0.055 W/W), GR_KCOR ranges from 32 to 124 GAPI, SIGF ranges from 13.3 to 40.2 CU and HTHO ranges from 4.0 to 15.1 ppm.
- The occurrence of siderite, iron-oxide or hydroxide is typical for these formations: a wide separation in the density-neutron, high total and spectral GR (especially HTHO and HURA that reached as high as 24.8 ppm and 4.5 ppm, respectively), high iron concentration (DWFE: above 0.055 W/W) and high PEFZ (up to 7.2 B/E).
- The matrix mineralogy is dominated by calcite with a siliciclastic component: in the lowest clay zones the PEFZ is in the range of 2.9 B/E to 5.7 B/E, while the calcium is relatively high (DWCA: up to 0.24 W/W; 0.394 W/W in pure calcite) and the DWSI is not negligible (mean = 0.21 W/W), which is typical of limestones and marls. In the Wedelsandstein Formation, the separation between the density-neutron is almost absent despite some clay being present, an indication that siliciclastics such as quartz are dominant. This is also indicated by the intermediate to high DWSI (up to 0.32 W/W) and the absence of correlation between clay content and silicon, which shows that the silicon is not primarily related to the clays.
- The spectral GR potassium (HFK) and thorium (HTHO) logs suggest the presence of both non-potassic (e.g. kaolinite, smectite) and potassic (e.g. illite) clay minerals.

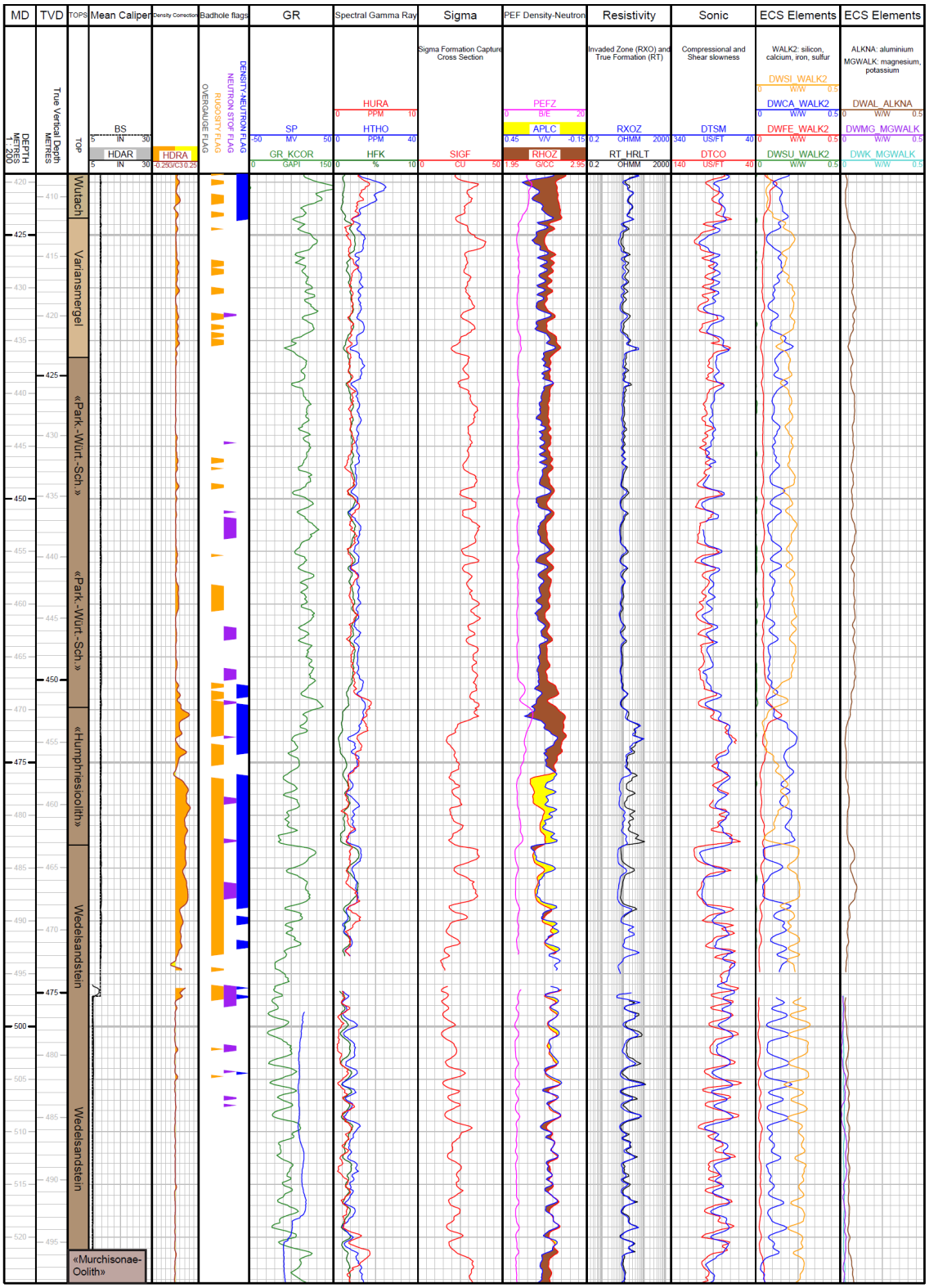

Fig. 3-3: Main logs of the composite dataset in the Wutach Formation to «Murchisonae-Oolith Formation»

3.4.4 Opalinus Clay (524.33 m to 668.19 m MD)

The top Opalinus Clay is characterised by an increase in clay content, as observed by the increase in total GR (GR_KCOR) and sigma (SIGF) and decrease in calcium concentration (DWCA), as well as a transition to more homogenous log signatures.

Log responses reflect the borehole lithology well because hole conditions were excellent for wireline logging. In the Opalinus Clay, logs have the following attributes (Fig. 3-4):

- Consistently intermediate to high clay content: the GR_KCOR ranges from 63 to 113 GAPI; SIGF correlates very well (positively) to GR_KCOR, ranging from 24.8 to 48.4 CU; the compressional wave slowness DTCO is high (slow formation) and generally above 91 µs/ft; the density-neutron separation is typical of lithologies with high clay content.
- Several carbonate streaks can be observed at 531.90 m, 536.50 m, 539.00 m, 540.10 m, 548.20 m, 553.40 m, and 554.40 m MD characterised by: an increase in density and decrease in neutron, with values approaching those of pure calcite (RHOZ: 2.71 g/cm^3; APLC: 0.0 v/v), an increase in calcium (DWCA up to 0.15 W/W) and an increase in resistivity logs (e.g. RT_HRLT).
- While the clay content is relatively homogeneous throughout, two distinct trends are observed. In the upper part of the formation, above 582.50 m MD, the clay content varies with carbonate content and generally remains lower than in the lower Opalinus Clay. Below 582.50 m MD, the clay content increases slightly with depth, as indicated by the gradual widening of the density-neutron separation and the increase in SIGF. Carbonate streaks are absent in the lower part of the formation.
- Matrix mineralogy is complex. Both calcium (DWCA) and silicon (DWSI) concentrations are often higher than those in smectite clays (DWCA: 0.00 to 0.14 W/W; DWSI: 0.16 to 0.29 W/W, excluding the carbonate streaks), which suggests siliciclastic and carbonate components in the matrix.
- The spectral GR potassium (HFK) and thorium (HTHO) logs suggest the presence of both non-potassic (e.g. kaolinite, smectite) and potassic (e.g. illite) clay minerals.

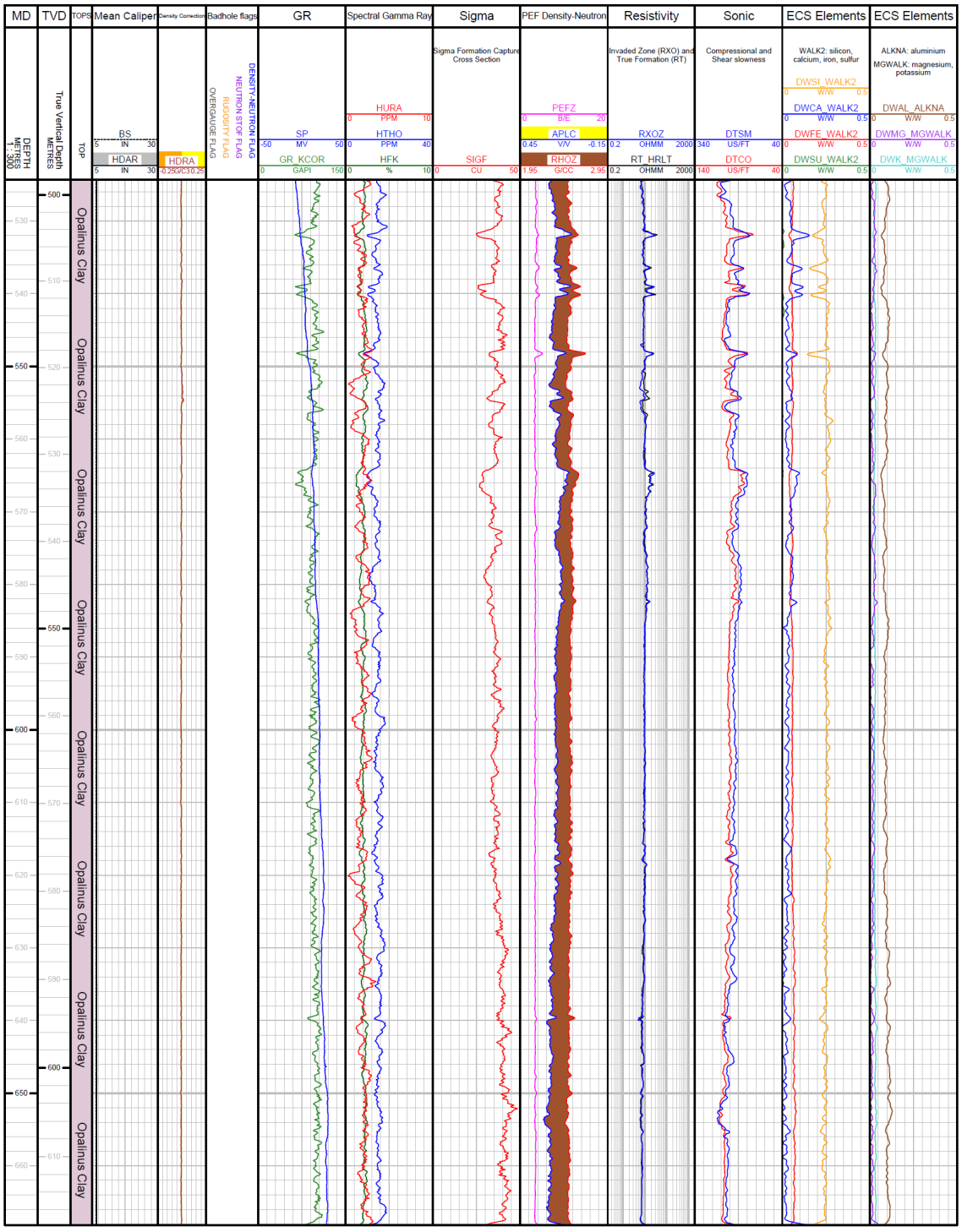

Fig. 3-4: Main logs of the composite dataset in the Opalinus Clay

3.4.5 Staffelegg Formation (668.19 m to 721.50 m MD)

The top of the Lias (Staffelegg Formation) can be identified by a decrease in total GR (GR_KCOR) and sigma (SIGF), a narrower separation in the density-neutron logs in a limestone-compatible scale and an increase in calcium contents (DWCA) (Fig. 3-5).

Hole conditions were good in the Staffelegg Formation. Logs respond well to the borehole lithology having the following attributes:

- Highly variable clay content: GR_KCOR (38 to 140 GAPI, excluding the organic matter), SIGF (14.6 to 45.8 CU) and HTHO (4.0 to 18.0 ppm), e.g. low clay content in the Breitenmatt Member, the Rickenbach Member and the Grünschholz Member (687.90 m to 692.98 m MD) but intermediate to high clay content in the Frick Member (692.98 m to 709.23 m MD).
- Organic matter is likely present: the high total GR zones (GR_KCOR > 107 GAPI, up to 157 GAPI) correspond with the uranium peaks (HURA: up to 17.0 ppm) in the Breitenmatt Member, the Rickenbach Member, the Grünschholz Member and the Beggingen Member.
- Pyrite is an important accessory mineral throughout the Staffelegg Formation: ECS sulphur dry weight fraction (DWSU) ranges from 0 to 0.03 W/W and the PEFZ, a reactive marker of pyrite, reaches a high value of 5.7 B/E.
- Matrix mineralogy is dominated by carbonates: calcium (DWCA) varies between 0 and 0.32 W/W (pure calcite: 0.394 W/W); however, mineralogy remains complex. The multi-mineral interpretation will help to better understand this complex mineralogy.
- The spectral GR potassium (HFK) and thorium (HTHO) logs suggest the presence of both non-potassic (e.g. kaolinite, smectite) and potassic (e.g. illite) clay minerals.

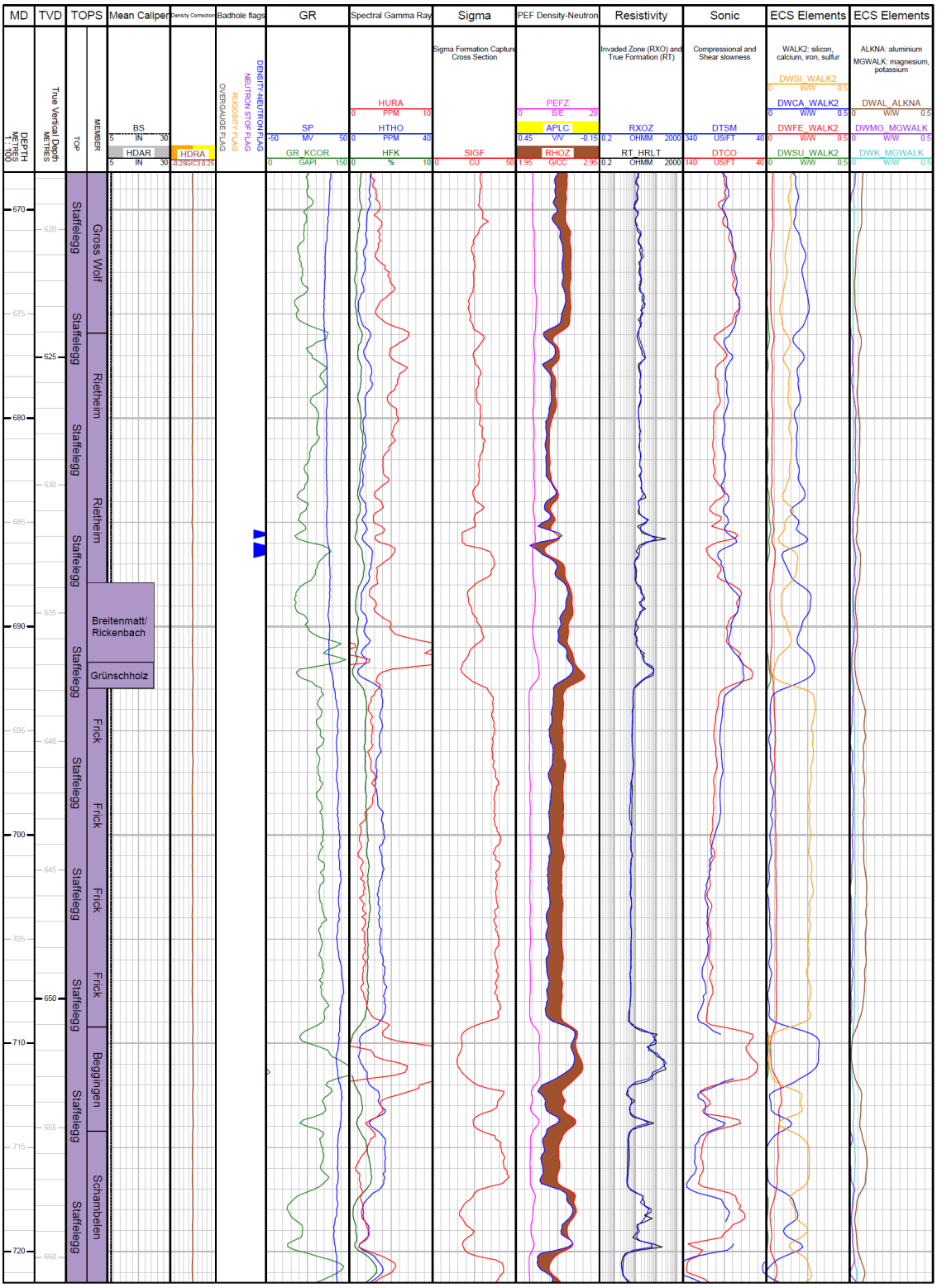

Fig. 3-5: Main logs of the composite dataset in the Staffelegg Formation

3.4.6 Klettgau Formation (721.50 m to 776.79 m MD)

The top of the Klettgau Formation is characterised by the appearance of dolomitic carbonates (replacing the calcium carbonates of the overlying Staffelegg Formation), indicated by the sharp increase in magnesium (DWMG) and a general decrease in the clay content indicators (e.g. GR_KCOR, SIGF) and clastic content (DWSI).

Hole conditions were good in the Klettgau Formation. Logs respond well to the borehole lithology having the following attributes (Fig. 3-6):

- Highly variable clay content: total GR ranges from ranges from 0 to 164 GAPI, sigma from 8.2 to 44.6 CU and thorium from 0 to 17.1 ppm; clay indicators have a bimodal distribution that reflects zones with low clay content (Seebi Member and Gansingen Member) and zones with moderately low to intermediate clay content (Gruhalde Member and Ergolz Member).
- Carbonate is the main matrix mineral in the Seebi Member and the Gansingen Member, as indicated by the intermediate to high calcium concentration (DWCA: 0.04 to 0.39 W/W; mean = 0.29 W/W; pure calcite: 0.394 W/W). The carbonate has a dolomitic signature, as shown by the PEFZ, with a mean value (3.7 B/E) close to that of pure dolomite (3.1 B/E), and ECS magnesium concentration (DWMG: 0.09 W/W).
- In the Gruhalde Member, the calcium and silicon concentrations are intermediate (mean DWCA: 0.14 W/W; mean DWSI: 0.18 W/W) and they are only loosely correlated with the clay content, indicating a mixed matrix mineralogy.
- In the Ergolz Member the calcium concentration is low (mean DWCA: 0.06 W/W) and the silicon concentration increases up to 0.31 W/W. This is also true for the zones with low clay content and suggests that the matrix mineralogy is dominated by siliciclastic minerals such as quartz.
- Organic matter is likely present, particularly at the base of the formation: the HURA increases up to 5.8 ppm in the lower Ergolz Member.
- The spectral GR potassium (HFK) and thorium (HRHO) logs suggest the presence of both non-potassic (e.g. kaolinite, smectite) and potassic (e.g. illite) clay minerals in the clay-rich zones.

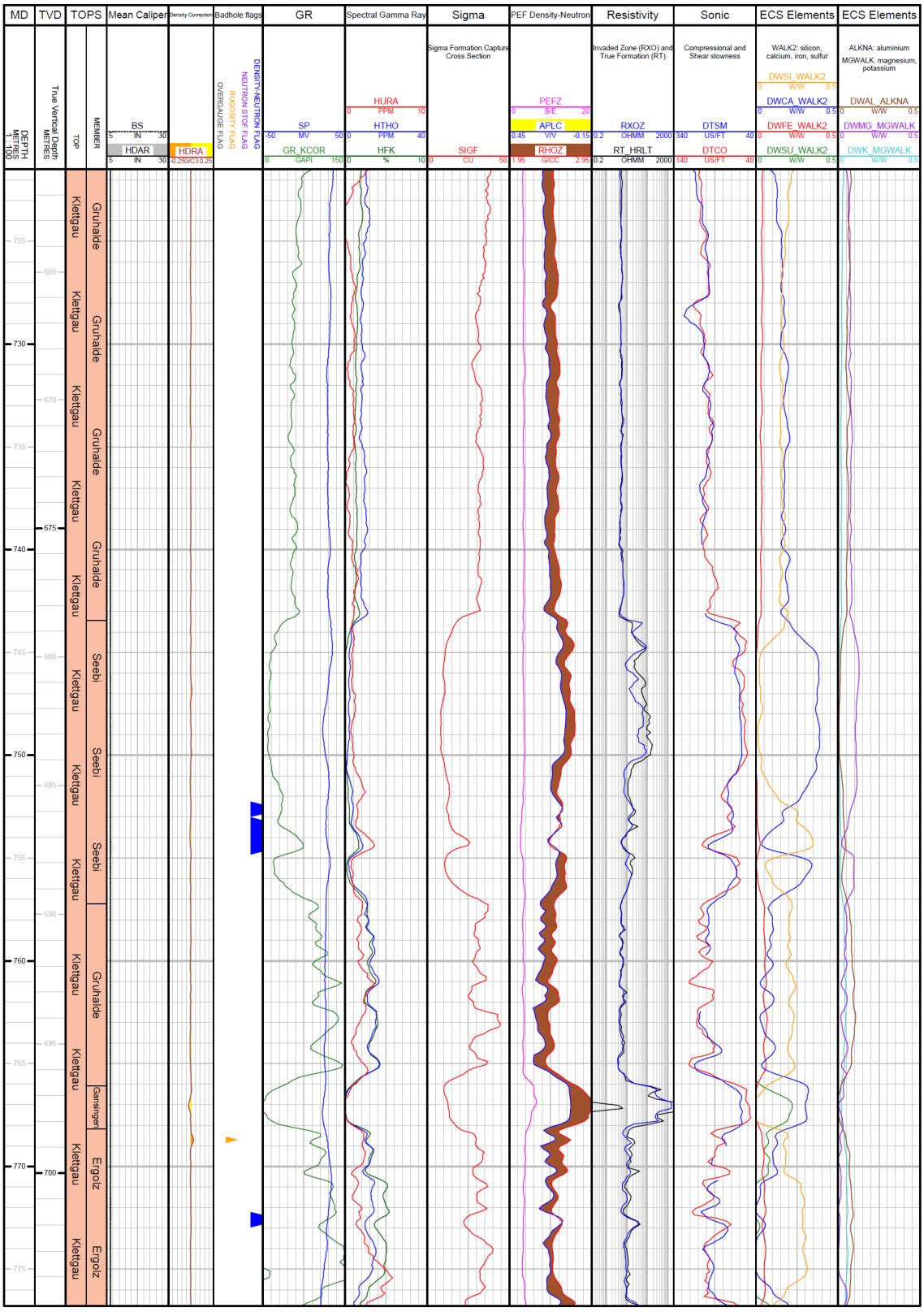

Fig. 3-6: Main logs of the composite dataset in the Klettgau Formation

3.4.7 Bänkerjoch Formation (776.79 m to 828.24 m MD)

The top of the Bänkerjoch Formation is characterised by an increase in evaporite (DWSU) and clay content (GR_KCOR, density-neutron separation) and decrease in clastic content (DWSI), associated with the transition from the silty-dominated lithology of the Ergolz Member to the anhydrite/claystone deposits of the Bänkerjoch Formation.

Hole conditions were generally good in the Bänkerjoch Formation, except for some borehole wall rugosity in the lower half of the formation. Logs respond well to the lithology having the following attributes (Fig. 3-7):

- Rapid variations in most logs at the metre scale or less from 808.60 m MD to TD (824.24 m MD), which suggest two main alternating lithologies. One having high sulphur (DWSU: up to 0.20 W/W) and calcium concentrations (DWCA: up to 0.28 W/W), high photoelectric factor (PEFZ: up to 5.0 B/E) and intermediate to low total GR, which suggest predominantly anhydrite bearing beds. The alternating beds have a higher clay content as indicated by the lower sulphur and calcium concentrations and intermediate to high sulphur concentrations (DWSI: up to 0.17 W/W) and total GR.
- The density-neutron separation (displaced in the limestone compatible scale) remains similar for both lithologies, but the logs shift from left to right for the clay and anhydrite dominant endmembers, respectively.
- Below 808.60 m MD, the lower Bänkerjoch Formation contains extended massive anhydrite beds, as indicated by consistently high DWSU (up to 0.20 W/W) and DWCA (up to 0.25 W/W), while clay content indicators remain low (e.g. GR_KCOR).
- Due to the limited vertical resolution of the logging tool, often higher than 10" (e.g. APS: 14"), the alternating lithologies are not necessarily correctly reflected in the logs. The logging tools average the physical and chemical properties over a fixed volume, which means that centimetre scale beds are represented as a mixture of anhydrite and clays for a given depth.
- The spectral GR potassium (HFK) and thorium (HTHO) logs suggest the presence of both non-potassic (e.g. kaolinite, smectite) and potassic (e.g. illite) clay minerals in the clay-rich zones.

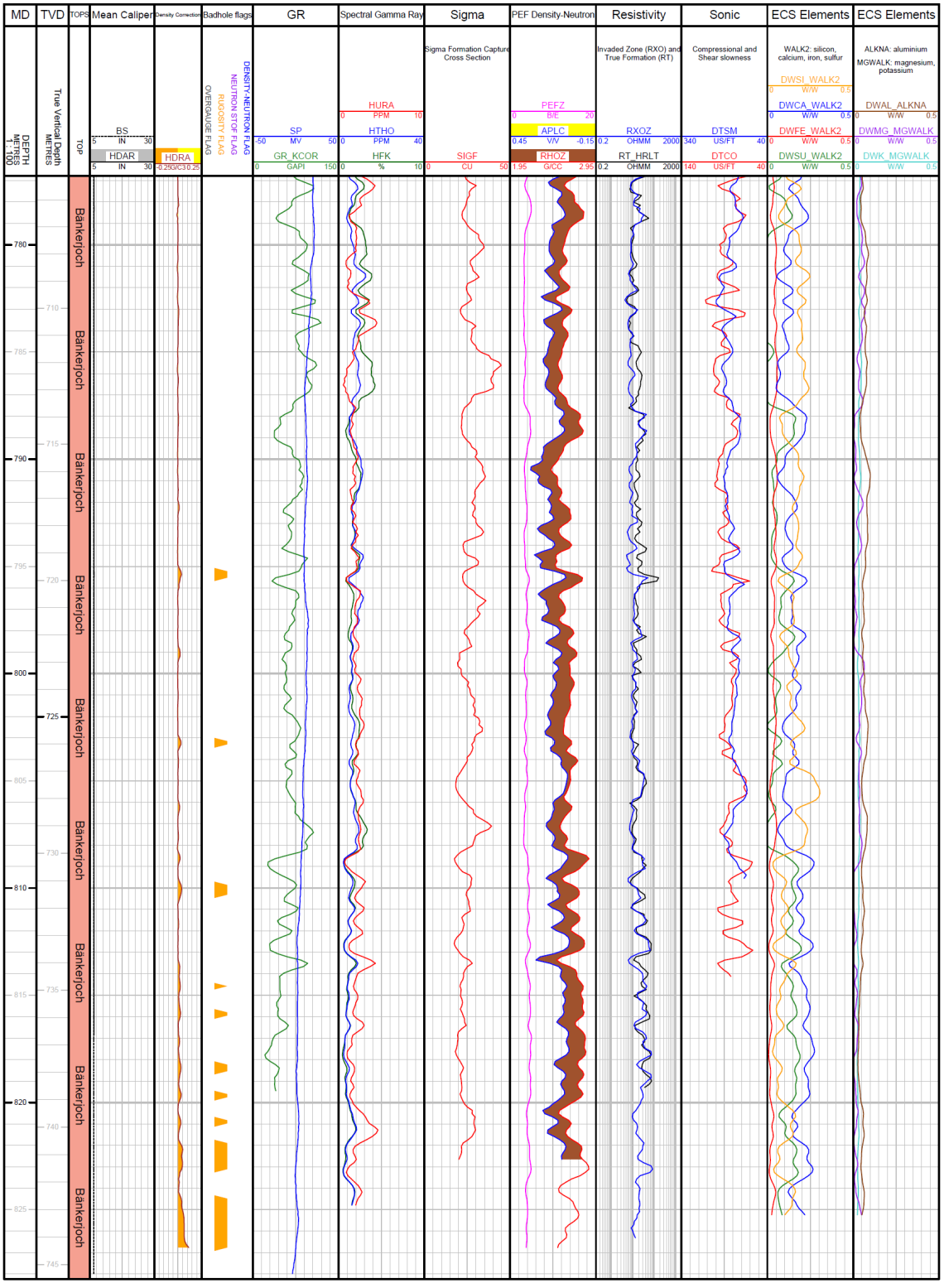

Fig. 3-7: Main logs of the composite dataset in the Bänkerjoch Formation

4 Borehole Imagery (BHI)

Borehole imaging tools produce high resolution circumferential images of the borehole wall by measuring either resistivity with tool pad contact or ultrasonic velocity. For the RHE1-1 borehole, SLB's Fullbore Formation MicroImager (FMI) and Ultrasonic Borehole Imager (UBI) were used. The FMI comprises of four pads that measure the formation resistivity via an array of buttons (24 per pad) that are pressed against the borehole wall, providing a vertical resolution of 2.5 mm and 80% coverage in an 8" hole diameter. The UBI has a rotating sub that sends out acoustic pulses to the formation and measures the amplitude and travel time of the returning signals, providing 5 mm vertical resolution and 100% borehole coverage. In general, fractures, faults and bedding are more easily identifiable using the FMI than the UBI as the microresistivity images provide better contrast. However, borehole wall features can be missed if they are located in an area not covered by the tool pad, which is why FMI and UBI images should be used together for image interpretation. In addition, breakouts are typically poorly resolved on microresistivity images because fracturing and spalling associated with these breakouts result in poor contact of the tool pads with the borehole wall.

BHI was used to:

- identify and characterise geological, sedimentological and structural features including bedding, fault planes / zones and fractures
- identify stress-induced borehole phenomena such as tensile drilling-induced fractures and breakouts
- perform core goniometry

In Fig. 4-1, the workflow used by NiMBUC Geoscience is described. Final processed and spliced image logs are included in Dossier V (Appendix B and Appendix C).

Step 1: Image QC	
Depth matching	Correlate high resolution image with reference GR
Caliper check	Verify calibration with casing ID, identify if borehole conditions could affect image quality (washouts, mud cake etc.)
Hardware check	Identify if downhole equipment performance indicators such as gain and voltage supply are consistent
Orientation check	Ensure orientation data are in agreement with borehole azimuth and deviation from independent survey
Accelerometer check	Accelerometer measurement should be consistent with earth's gravity (1 g = 9.81 ± 0.03 m/s^2)
Magnetometer check	Magnetometer consistent with theoretical magnetic field strength at location, X-Y magnetometers behave complementary, QC magnetic declination parameters input
Tool movement check	Identification of any stick and pull events using tension and accelerometer measurements
Acquisition check	Verify frame time and cable speed control
Borehole image check	Identification of dead buttons or pads and any casing interference

Step 2: Image processing	
Basic image generation	Azimuthal orientation of images to true or grid north
	Merging of individual tool run passes
	Splicing of data between drilling sections
	If required, invert images to ensure per industry standards that low value = low resistivity and high value = high resistivity
	If required, correct offsets between pad images
	Bad button detection and correction
Image equalisation and normalisation	Static normalisation involving selecting the normalisation distribution (uniform/Gaussian), equalisation strength, high/low cut-offs for equalisation etc.
	Dynamic normalisation to enhance local contrasts highlighting features in a selected sliding window of a few metres

Step 3: Basic interpretation	
Manual picking of features directly from the processed image in accordance with Nagra classification scheme detailed here	Drilling-induced fractures
	Borehole breakouts
	Bedding
	Fractures (conductive, partially conductive, resistive, partially resistive, faint trace)
	Faults (conductive, partially conductive, resistive, partially resistive, faint)

Fig. 4-1: Borehole image processing workflow

5 Micro-hydraulic Fracturing (MHF)

5.1 Introduction and objectives

A series of stress measurements were planned in the RHE1-1 borehole using the Micro-hydraulic Fracturing (MHF) technique. MHF testing in boreholes is the only direct method available for measuring rock stress magnitude at great depth. An overview of the methodology can be found in Haimson (1993), Desroches & Kurkjian (1999) and Haimson & Cornet (2003) and references therein. Recent updates on the methodology, some of which having been specifically designed for this project, can be found in Desroches et al. (2021a, 2021b).

The objectives of the testing programme in RHE1-1 were to acquire data to:

- assess if the presence of a discontinuity in the Opalinus Clay induced any changes in the stress field
- confirm if the in situ state of stress in the formations intersected by RHE1 1 is similar to that of the other boreholes in the Zürich Nordost siting region (Marthalen-1-1 and Trüllikon-1-1)
- provide calibration points for mechanical earth models (MEM) of the rock mass (1D, 3D). See Bérard & Prioul (2016) for an overview of mechanical earth models and Plumb et al. (2000) for a definition of an MEM.

5.2 MHF testing feasibility in the Opalinus Clay

In a vertical borehole, a hydraulic fracture typically initiates along the "preferred fracture plane", perpendicular to the far-field minimum principal stress. In a deviated borehole (Fig. 5-1), the behaviour is often different: a hydraulic fracture typically initiates away from the preferred fracture plane and gradually reorients towards it as it grows away from the borehole (e.g. Weijers 1994, for an extensive study of this phenomenon). The angle between the initial fracture trace at the borehole wall and the preferred fracture plane is referred to as the reorientation angle χ in this report. A schematic of possible cases for vertical and horizontal boreholes is presented in Fig. 5-2. Note that herein it is assumed that the vertical stress is a principal stress, which is a typical assumption for the state of stress at depth.

To be able to measure the far-field minimum stress from an MHF test, χ should be less than 30°. If it is larger than 30°, a large portion of the created fracture is not exposed to the far-field minimum stress and might exhibit artefacts during both fracture closure and fracture reopening. Furthermore, instead of initiating as a two-wing axial fracture, the hydraulic fracture can form an 'en échelon' configuration (multiple segments inclined with respect to the borehole axis), which is detrimental to fracture reorientation and can be quantified with the angle ω between the fracture trace at the borehole and the borehole axis, which will be referred to as the en-échelon angle in this report.

It is preferable for ω to be small, typically less than 15°, otherwise the various segments created at the borehole wall typically only merge far away or not at all from the borehole wall. Interaction between the segments reduces the fracture reorientation towards the far-field preferred fracture plane so that the MHF test does not probe the far-field stress (e.g. Weijers & de Pater 1994 and Weijers 1994, for an in-depth description of this phenomenon). The values of χ and ω depend not only on the properties of the formation, but also on the azimuth and deviation of the borehole, as well as the complete far-field stress tensor (direction and magnitudes).

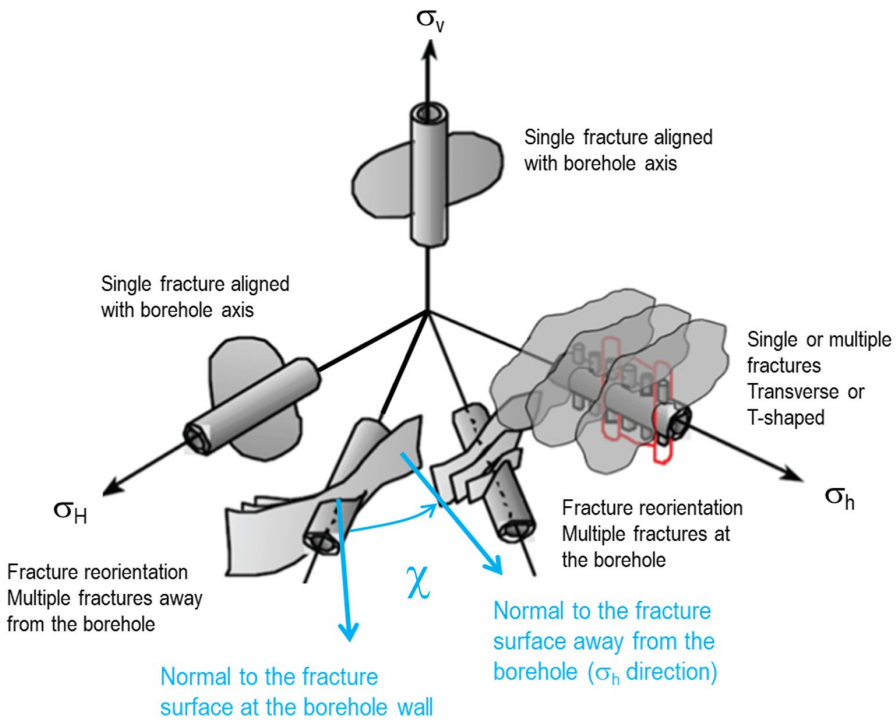

Fig. 5-1: Typical fracture geometry at the borehole wall and away from the borehole as a function of borehole azimuth with respect to far-field stress directions

σ_v is the vertical stress, σ_h is the minimum horizontal stress and σ_H is the maximum horizontal, all of which are assumed to be principal stresses. θ is the angle between σ_H and the borehole and χ is the reorientation angle defined as the angle of rotation between the normal of the fracture at the borehole wall and the direction of the minimum horizontal stress.

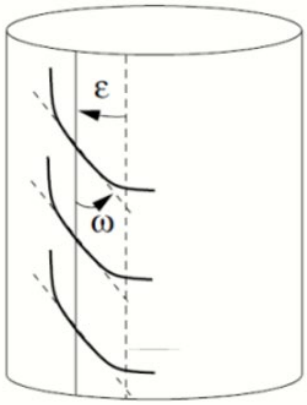

Fig. 5-2: Angles characterising 'en-échelon' fracture geometry at the wall of a deviated borehole

ε is the angle from the middle of the en-échelon segments to the top of hole and ω is the angle of the segments in relation to the borehole axis.

Due to the likelihood of encountering conveyance problems with the Modular Formation Dynamics Tester (MDT) in RHE1-1, it was decided to restrict the scope of MHF testing to the Opalinus Clay. A modelling assessment of the influence of the borehole trajectory on the initial geometry of a hydraulic fracture was performed to ensure that an MHF test could be interpreted with confidence to determine far-field stress values, i.e. resulting in angles χ and ω smaller than 30° and 15°, respectively.

Using a realistic range of values for both the formation parameters and the far-field stress state, the orientation of the initial trace of the fracture at the borehole wall was studied with Schlumberger's Stress Test Planner (STP). Based on existing stress measurements already acquired in the Opalinus Clay during the TBO campaign, it was assumed that the minimum stress would be the far-field minimum horizontal stress σ_h. An analytical model was used to compute the geometry of a hydraulic fracture at a borehole wall as well as the likely initiation pressure (note that the geometry depends on the initiation pressure). A priori distributions of formation parameters, far-field stress and borehole azimuth and deviation were sampled to reconstruct probability density functions of angles χ and ω to provide a description of the fracture that would have likely been generated by an MHF test in the Opalinus Clay of RHE1-1. More details on STP for deviated boreholes can be found in Bérard et al. (2019).

An initial analysis considered all possible borehole deviations and azimuths. Fig. 5-3 presents the results of the analysis for the en-échelon angle ω as a function of borehole azimuth A_w and deviation D_w for the range of parameters considered (e.g. formation tensile strength, horizontal stress ratio). Fig. 5-4 presents the results of the same analysis for the reorientation angle χ.

The results of the global analysis show that the average en-échelon angle ω is typically less than 15° (Fig. 5-3a and c) and thus acceptable. If the borehole deviation is less than 35°, the average fracture reorientation angle χ is less than 30° (Fig. 5-4a) and thus appears acceptable. The probability distribution of χ (Fig. 5-4c) shows two distinct behaviours, one close to 0° and the other spanning a range from 0 to 90° as a function of borehole azimuth. Some of the combinations of the considered parameters clearly yielded reorientation angles outside of the acceptable range of 0 to 30°, even if the average did not. This observation led to a refined investigation focused on the azimuth and deviation of the RHE1-1 borehole expected in the Opalinus Clay (azimuth close to that of σ_h and deviation around 38°).

a)

b)

c)

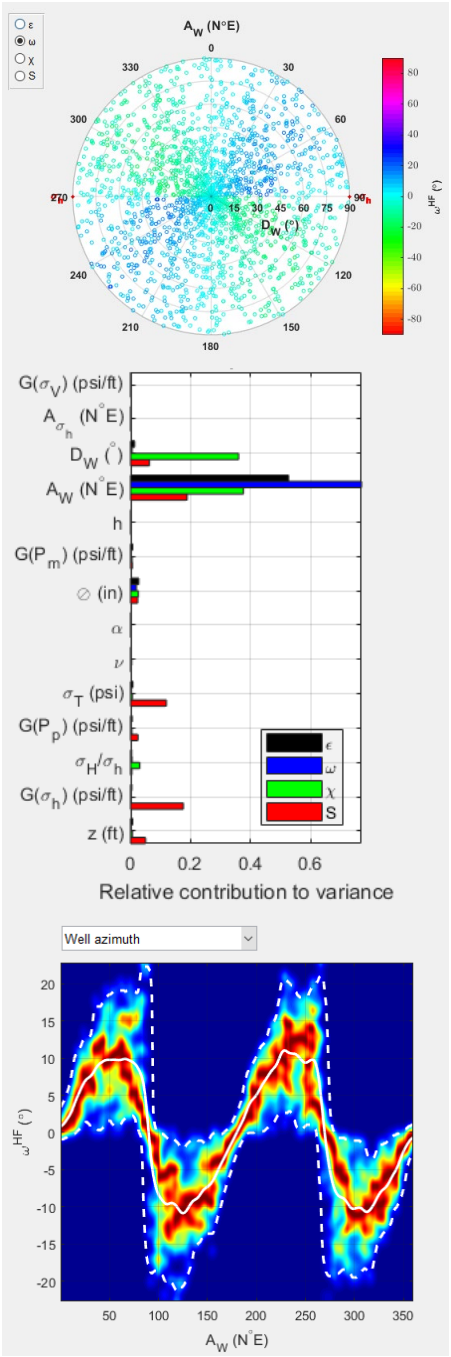

Variance diagram legend

$G(\sigma_V)$	Gradient of vertical stress
A_{σ_h}	Azimuth of minimum horizontal stress
D_W	Borehole deviation
A_W	Borehole azimuth
h	Mud cake coefficient
$G(P_m)$	Gradient of formation pore pressure
$\emptyset$(in)	Borehole diameter
α	Biot's poroelastic parameter
υ	Poisson's ratio
σ_T	Tensile strength of formation
$G(P_p)$	Formation pore pressure gradient
σ_H/σ_h	Ratio of maximum to minimum horizontal stress
$G(\sigma_h)$	Gradient of minimum horizontal stress
z(ft)	Depth

Fig. 5-3: Fracture initiation analysis showing the en-échelon angle ω for σ_h azimuth N90E and any borehole trajectory

a) polar plot of ω for each borehole azimuth A_w and deviation D_w; b) variance diagram showing the relative contribution of all input parameters to the variance of angles ε in black, ω in blue, χ in green and the fracture initiation pressure S in red. The larger the variance the more effect the corresponding parameter has on the output. For example, A_w has the largest influence on the variation of ω; c) probability density plot of ω as a function of A_w, where the average is indicated by the solid white line, the 95th percentiles by the white dashed lines and the density colormap showing low and high occurrence with dark blue and dark red, respectively. For example, for a borehole azimuth of N50E, the 95th percentile range for ω is 2 to 20° with an average of 10°.

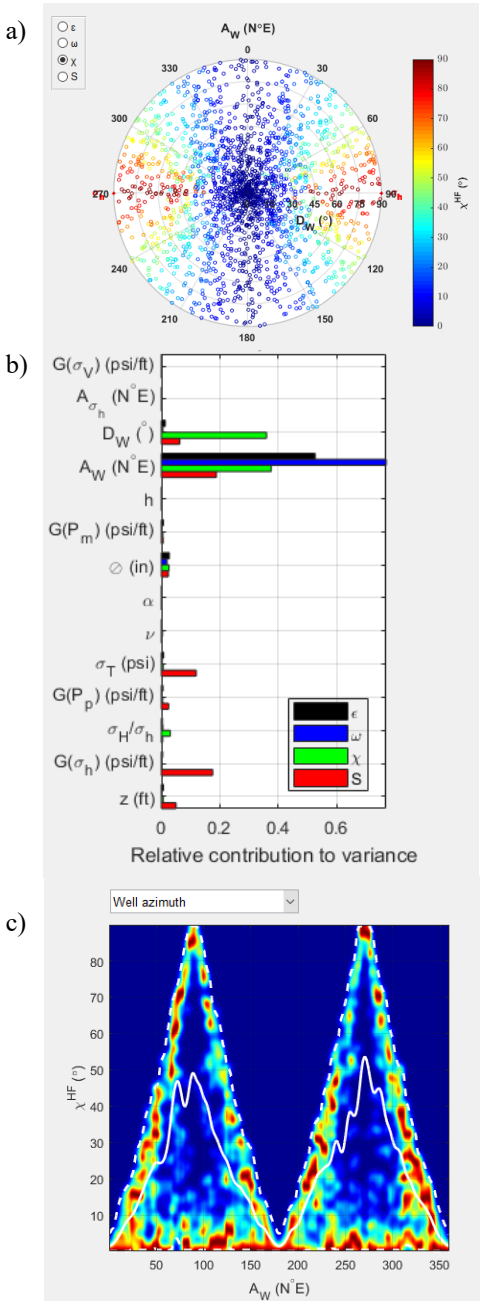

Variance diagram legend

$G(\sigma_V)$	Gradient of vertical stress
A_{σ_h}	Azimuth of minimum horizontal stress
D_W	Borehole deviation
A_W	Borehole azimuth
h	Mud cake coefficient
$G(P_m)$	Gradient of formation pore pressure
$\emptyset$(in)	Borehole diameter
α	Biot's poroelastic parameter
υ	Poisson's ratio
σ_T	Tensile strength of formation
$G(P_p)$	Formation pore pressure gradient
σ_H/σ_h	Ratio of maximum to minimum horizontal stress
$G(\sigma_h)$	Gradient of minimum horizontal stress
z(ft)	Depth

Fig. 5-4: Fracture initiation analysis showing the reorientation angle χ for σ_h azimuth N90E and any borehole trajectory

a) polar plot of χ for each borehole azimuth A_w and deviation D_w; b) variance diagram showing the relative contribution of all input parameters to the variance of angles ε in black, ω in blue, χ in green and the fracture initiation pressure S in red. The larger the variance the more effect the corresponding parameter has on the output. For example, A_w and D_w have the largest influence on χ. The variance diagram is the same as that of Fig. 5-3 as the analysis is the same; c) probability density plot of χ as a function of A_w, where the average is indicated by the solid white line, the 95th percentiles by the white dashed lines and the density color-map showing low and high occurrence with dark blue and dark red, respectively. For example, for a borehole azimuth of N50E, the 95th percentile range of χ is 0 to 45° with an average of 25°. The distribution, however, comprises of two peaks highlighted in red, one close to 0° and the other spanning 30 to 40°.

The results of the focused analysis show that two potential behaviours also appear for the en-échelon angle ω, with values alternating between 0° and 20° (Fig. 5-5c and d). Around 38° of deviation, both values appear equally probable, indicating that a small change in the formation parameters or stresses will trigger a large change in ω. It is worth remembering that a value of 20° falls outside if the desired range of ω.

The two potential behaviours, already seen for the reorientation angle χ are confirmed in the focused analysis, with values either typically lower than 20° or higher than 70° (Fig. 5-6c and d). There is a transition zone where both behaviours are possible for a borehole deviation between 37° and 42° (Fig. 5-6d), within which lies the deviation of RHE1-1 in the Opalinus Clay.

As a result, for the borehole conditions encountered in RHE1-1, the initial fracture orientation described by angles ω and χ is expected to be unpredictable as two different modes are equally probable. Furthermore, one of these modes is outside of the limits for interpretation ($\omega < 15°$ and $\chi < 30°$), meaning that MHF results would be unlikely to yield σ_h values.

Testing an adequately oriented drilling enhanced feature (vertical and perpendicular to σ_h) would solve the problem highlighted above, because it is easier to propagate a feature exposed to the far-field principal stress than to create a new feature. However, no such feature was observed in the FMI and UBI logs.

As a consequence, no MHF was attempted in the RHE1-1 borehole.

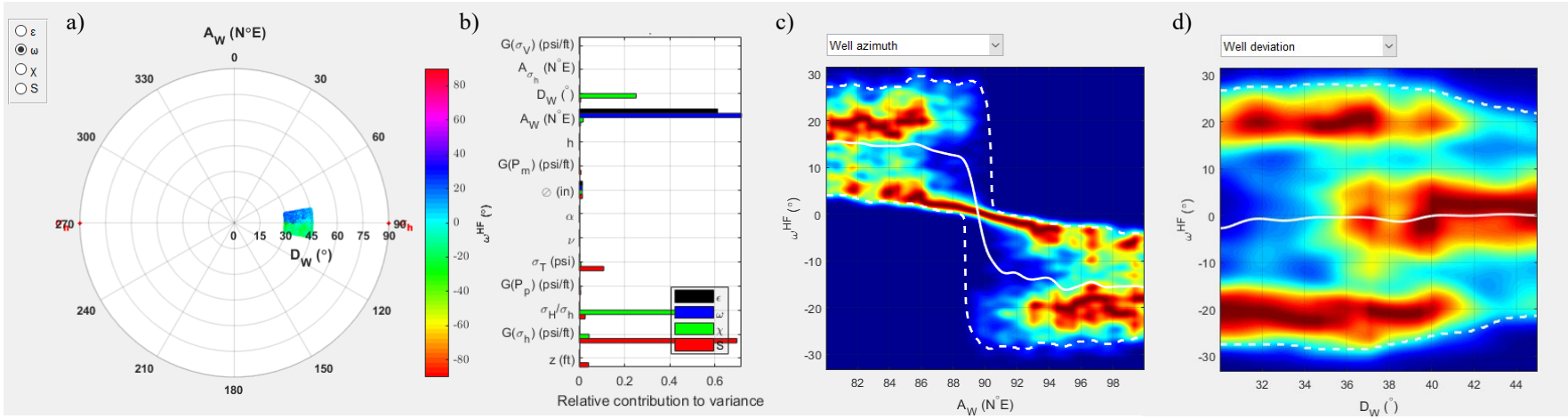

Fig. 5-5: Focused fracture initiation analysis showing the en-échelon angle ω for σ_h azimuth N90E, for the azimuth A_w and deviation D_w expected in the RHE1-1 borehole in the Opalinus Clay formation: A_w within ± 10° of σ_h, deviation between 30 and 45°

a) polar plot showing small variations of the average ω for each borehole A_w and D_w; b) variance diagram indicating which parameter has the most influence on the results – see Fig. 5-3 for a definition of the parameters. For example, A_w has the largest influence on the variation of ω; c) and d) probability density function of ω as a function of A_w and D_w, respectively, with the average indicated as a solid white line, 95th percentiles by the white dashed lines and density colormap showing low and high occurrence with dark blue and dark red, respectively.

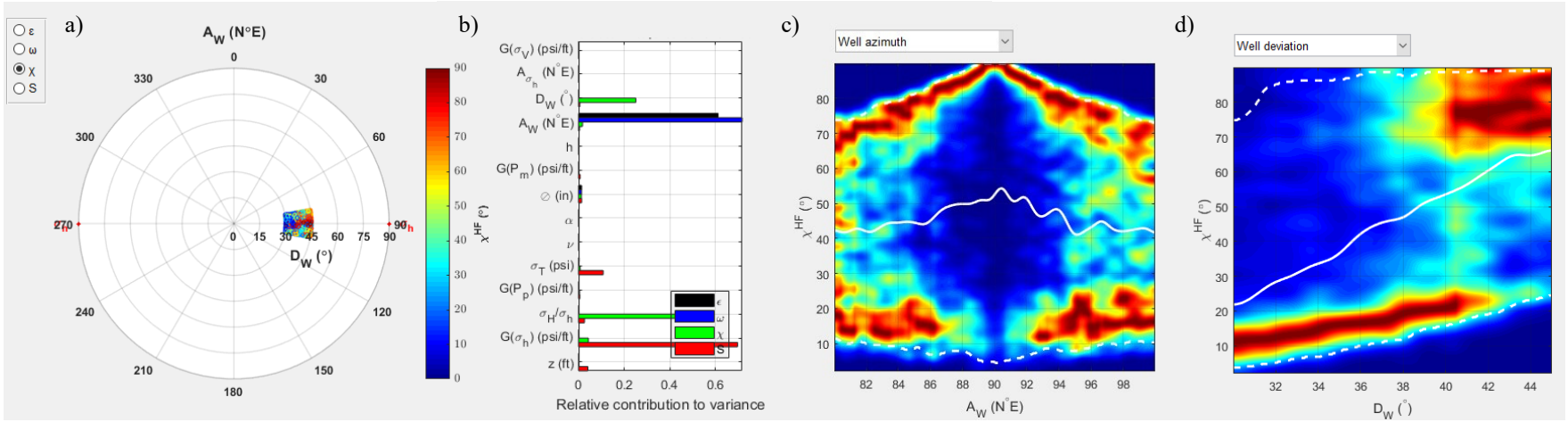

Fig. 5-6: Focused fracture initiation analysis showing the reorientation angle χ for σ_h azimuth N90E, for the azimuth A_w and deviation D_w expected in the RHE1-1 borehole in the Opalinus Clay: A_w within ± 10° of σ_h, deviation between 30 and 45°

a) polar plot showing the average χ for each borehole A_w and D_w – nearly complete spectrum of possible angles shown in the small sector indicating unstable behaviour; b) variance diagram indicating which parameter has the most influence on the results – see Fig. 5-3 for a definition of the parameters. For example, σ_H/σ_h and D_w have the largest impact on χ. The variance diagram is the same as that of Fig. 5-5 as the analysis is the same; c) and d) probability density function of the angle χ as a function of A_w and D_w, respectively, with the average indicated as a solid white line, 95th percentiles by the white dashed lines and density colormap showing low and high occurrence with dark blue and dark red, respectively.

6 References

Bérard, T. & Prioul, R. (2016): Mechanical Earth Model. Oilfield Review: The Defining Series, https://www.slb.com/resource-library/oilfield-review/defining-series/defining-mem.

Bérard, T., Mishra, V.K., Cedillo, G., Pineda, W., Chugunov, N. & Prioul, R. (2019): Leveraging return of experience to improve the success rate of formation stress tests: a case study in the Gulf of Mexico. Paper ARMA 19-66 presented at the 53rd US Rock Mechanics/ Geomechanics symposium, New York, NY, USA, June 2019.

Birkhäuser, P., Roth, P., Meier, B. & Naef, H. (2001): 3D-Seismik: Räumliche Erkundung des mesozoischen Sedimentschichten im Zürcher Weinland. Nagra Technischer Bericht NTB 00-03.

Desroches, J. & Kurkjian, A.L. (1999): Applications of wireline stress measurements. Paper SPE-58086, SPE Reservoir Evaluation & Engineering 2/5, 451-461. DOI:10.2118/ 58086-PA.

Desroches, J., Peyret, E., Gisolf, A. Wilcox, A., Di Giovanni, M., Schram de Jong, A., Sepehri, S., Garrard, R. & Giger, S. (2021a): Stress measurement campaign in scientific deep boreholes: Focus on tool and methods. SPWLA Paper #2021-056 presented at the SPWLA 62nd Annual Logging Symposium, May 17-20 2021.

Desroches, J., Peyret, E., Gisolf, A., Wilcox, A., di Giovanni, M., Schram de Jong, A., Milos, B., Gonus, J., Bailey, E., Sepehri, S., Garitte, B., Garrard, R. & Giger, S. (2021b): Stress-measurement campaign in scientific deep boreholes: From planning to interpretation. ARMA-2-21-1928 presented at the 55th U.S. Rock Mechanics/Geomechanics Symposium, Virtual, June 2021.

Haimson, B.C. (1993): The hydraulic fracturing method of stress measurement: Theory and practice. *Chapter 14 in:* Hudson, J. (ed.): Comprehensive Rock Engineering 3, 395-412, Pergamon Press. DOI: 10.1016/B978-0-08-042066-0.500215.

Haimson, B.C. & Cornet, F.H. (2003): ISRM suggested methods for rock stress estimation – Part 3: Hydraulic Fracturing (HF) and/or Hydraulic Testing of Pre-Existing Fractures (HTPF). International Journal Rock Mechanics and Mining Sciences 40/7-8, 1011-1020. DOI: 10.1016/j.ijrmms.2003.08.002.

Isler, A., Pasquier, F. & Huber, M. (1984): Geologische Karte der zentralen Nordschweiz 1:100'000. Herausgegeben von der Nagra und der Schweiz. Geol. Komm.

Jäggi, D., Laurich, B., Nussbaum, C., Schuster, K. & Connolly, P. (2017): Tectonic structure of the "Main Fault" in the Opalinus Clay, Mont Terri rock laboratory (Switzerland). Swiss Journal of Geosciences 110, 67-84.

Nagra (2014): SGT Etappe 2: Vorschlag weiter zu untersuchender geologischer Standortgebiete mit zugehörigen Standortarealen für die Oberflächenanlage. Geologische Grundlagen. Dossier II: Sedimentologische und tektonische Verhältnisse. Nagra Technischer Bericht NTB 14-02.

Nagra (2019): Preliminary horizon and structure mapping of the Nagra 3D seismics ZNO-97/16 (Zürich Nordost) in time domain. Nagra Arbeitsbericht NAB 18-36.

Pietsch, J. & Jordan, P. (2014): Digitales Höhenmodell Basis Quartär der Nordschweiz – Version
Plumb, R., Edwards, S., Pidcock, G., Lee, D. & Stacey, B. (2000): The Mechanical Earth Model concept and its application to high-risk well construction projects. SPE Paper #59128 presented at the IADC/SPE Drilling Conference, New Orleans, Louisiana, February 2000. DOI: https://doi.org/10.2118/59128-MS.

Roche, V., Childs, C., Madritsch, H. & Camanni, G. (2020): Controls of sedimentary layering and structural inheritance on fault zone structure in three dimensions. A case study from the northern Molasse basin, Switzerland. Journal of the Geological Society 177/3, 493-508.

Weijers, L. (1994): Near-wellbore geometry of hydraulic fractures from deviated and horizontal wellbores. Doctoral dissertation, PhD thesis, Delft University Press.

Weijers, L. & de Pater, C.J. (1994): Interaction and link-up of hydraulic starter fractures close to a perforated wellbore. Paper presented at the Rock Mechanics in Petroleum Engineering, Delft, Netherlands, August 1994.